Accepted Manuscript

Journal of the Geological Society

The journey of the Band-e-Zeyarat ophiolite (Makran Accretionary Wedge, SE Iran) from the mid-ocean ridge to the accretionary complex: New insights from its sedimentary cover and associated basaltic dykes and sills

Edoardo Barbero, Luca Pandolfi, Morteza Delavari, Asghar Dolati, Emilio Saccani, Rita Catanzariti & Michele Marroni

DOI: https://doi.org/10.1144/jgs2023-043

To access the most recent version of this article, please click the DOI URL in the line above. When citing this article please include the above DOI.

This article is part of the Ophiolites, melanges and blueschists collection available at: https://www.lyellcollection.org/topic/collections/ophiolites-melanges-and-blueschists

Received 13 April 2023
Revised 28 August 2023
Accepted 30 August 2023

Supplementary material at https://doi.org/10.6084/m9.figshare.c.6843835

The journey of the Band-e-Zeyarat ophiolite (Makran Accretionary Wedge, SE Iran) from the mid-ocean ridge to the accretionary complex: New insights from its sedimentary cover and associated basaltic dykes and sills

Short title: Band-e-Zeyarat ophiolite sedimentary cover

Edoardo Barbero [1*], Luca Pandolfi [2,3], Morteza Delavari [4], Asghar Dolati [4], Emilio Saccani [5], Rita Catanzariti [3], and Michele Marroni [2,3]

1 Istituto di Geoscienze e Georisorse, CNR, Torino, Via Valperga Caluso 35, 10125 Torino, Italy

2 Dipartimento di Scienze della Terra, Università di Pisa, Via S. Maria 53, 56126 Pisa, Italy

3 Istituto di Geoscienze e Georisorse, CNR, Pisa, Via G. Moruzzi 1, 56124 Pisa, Italy

4 Faculty of Earth Sciences, Kharazmi University, Shahid Mofatteh St. 43, Tehran, Iran

5 Dipartimento di Fisica e Scienze della Terra, Università di Ferrara, Via Saragat 1, 44123 Ferrara, Italy

*Correspondence: edoardobarbero91@gmail.com

Abstract

The Band-e-Zeyarat ophiolite (BEZO) sedimentary cover in the Makran Accretionary Prism (SE Iran) records a complex tectono-sedimentary evolution, extending from its formation at a mid-ocean ridge setting to deformation in an accretionary prism. Stratigraphic and biostratigraphic data indicate the occurrence of a Valanginian transition zone sequence separating the volcanic sequence and pelagic sedimentary cover. The latter consists of lower Hauterivian cherty limestone passing upwards to upper Hauterivian – Barremian marl and limestone. The pelagic sedimentary cover continues with post-Barremian – Cenomanian (?) marls. Arenites are interlayered in the sedimentary cover; they are composed of rock fragments derived from volcanic arc and continental margin settings. The BEZO sedimentary cover is intruded by dykes and sills showing enriched mid-ocean ridge (MOR) basalt chemical affinity. Structural analysis indicates a polyphase deformation history that involved faulting and folding. Our multidisciplinary results indicate that the BEZO formed in a MOR setting and that it was subsequently overprinted by off-axis and within-plate magmatism as it spread away from this MOR. The Band-e-Zeyarat oceanic crust was incorporated into the Makran prism in the latest Late Cretaceous – Paleocene, and was further deformed via strike-slip faulting along the dextral Minab-Sabzevaran fault during the Miocene - Pliocene.

Keywords: tectono-sedimentary evolution, stratigraphy, ophiolite sedimentary cover, Makran, Iran, Neo-Tethys.

Ophiolites represent fragments of upper mantle and oceanic crust incorporated into both collisional and accretionary belts during the closure of ancient oceanic basins (Dewey & Bird, 1971; Dilek and Furnes, 2011, 2014; Furnes and Dilek, 2021). They may originate in different oceanic settings such as ocean-continent transition zones, mid-oceanic ridges, supra-subduction zones, back-arc basins, and within-plate oceanic islands (Dilek and Furnes, 2011; Saccani et al., 2015; Furnes et al., 2020). The stratigraphic architecture of the crustal magmatic rocks, as well as their geochemical features show distinctive characteristics that are strongly dependent on their geodynamic setting of formation (e.g., Shervais, 2001; Dilek and Furnes, 2011; Pearce, 2008, 2014; Saccani, 2015). In contrast, the stratigraphic features of the sedimentary cover of the ophiolites are strongly influenced by the tectono-sedimentary evolution of the oceanic lithosphere during its journey from the original setting of formation to a trench and its incorporation into collisional or accretionary belts (e.g., Isozaki et al., 1990; Kusky et a., 2013; Wakita, 2015). Therefore, geochemical data on ophiolitic magmatic rocks coupled with stratigraphic data on the sedimentary cover are essential for the reconstruction of the journey of ancient oceanic lithosphere, from its setting of formation to its arrival at a convergent margin.

In the Makran Accretionary Prism (southern Iran and Pakistan; Figs. 1a, b), fragments of the Neotethyan oceanic lithosphere are preserved within the North Makran domain, which is the structurally uppermost tectono-stratigraphic domain of the prism. In the western sector of this domain, the Band-e-Zeyarat ophiolite (BEZO, Figs. 1c, d) is one of the best-exposed ophiolite complexes, composed of Lower Cretaceous oceanic crustal rocks overlain by a sedimentary cover (McCall, 1985; Kananian et al., 2001; Ghazi et al., 2004; Barbero et al., 2020a; Ghasemi Siani et al., 2021a, b). The latter represents a pelagic sequence consisting of cherty limestones passing to alternating limestones and marls, as well as intercalations of calcareous and siliciclastic turbidites (McCall, 1985). In addition, minor basaltic sills and dykes crosscut the sequence. The BEZO has been recently interpreted either as formed in a mid-ocean ridge tectono-magmatic setting (Barbero et al., 2020a) or in a back-arc setting (Ghasemi Siani et al., 2021b). Stratigraphic and structural data

on the sedimentary cover of this ophiolite can provide fundamental constraints to reveal the tectono-stratigraphic evolution of the oceanic lithosphere during the journey from the mid-ocean ridge to the incorporation within the Makran accretionary complex.

The aim of this paper is to discuss the tectono-sedimentary history of the sedimentary cover of the BEZO from its formation in the mid-ocean ridge setting to its deformation in the Makran Accretionary Prism. For these reasons, we present a multidisciplinary study on the sedimentary cover of the BEZO, including stratigraphic, biostratigraphic, and structural data, whole-rock geochemical data on dykes and sills, and petrographic characterization of arenites, which are interlayered with pelagic rocks in the sedimentary cover.

Geological setting

The Makran Accretionary Prism (Fig. 1b) has developed as a result of the convergence between the Arabian and Eurasian plates that has been accommodated by the northward subduction of the Neotethys oceanic lithosphere since the Cretaceous (McCall & Kidd, 1982; Dercourt et al., 1986; Glennie et al., 1990; Burg, 2018; Barrier et al., 2018; Khalili et al., 2022). From north to south (i.e., from the upper to the lower structural position) five tectono-stratigraphic domains have been distinguished in this prism, including the North, Inner, Outer, Coastal, and Off-shore Makran domains (Fig. 1b; Dolati, 2010; Burg et al., 2013; Dolati & Burg, 2013; Burg, 2018). Each domain is bounded by regional thrust faults (Fig.1b; Dolati, 2010) and is composed of tectono-sedimentary assemblages recording the progressive growth of the prism since the Late Cretaceous (Dolati, 2010; Burg et al., 2013; Burg, 2018; Barbero et al., 2020a, b, 2021a; Barbero et al., 2023; Pandolfi et al., 2021).

The North Makran domain was deformed during the pre-Eocene tectonic evolution of the accretionary wedge (McCall 1985; McCall & Kidd, 1982; Hunziker et al., 2015; Burg, 2018;

Barbero, 2021; Barbero et al., 2023). This domain is largely composed of: i) mid-ocean ridge- (MOR) and plume-type ophiolites (*sensu* Dilek and Furnes, 2011, 2014) with or without high pressure – low temperature metamorphism and ophiolitic mélanges; ii) volcanic arc sequences; iii) turbiditic successions (McCall, 1985, 1997; Hunziker et al., 2015, 2017; Saccani et al., 2018, 2022a, b; Burg, 2018; Esmaeili et al., 2019, 2020; Sepidbar et al., 2020; Barbero et al., 2020a, b, 2021a, b, 2023; Moghadam et al., 2022). The Bashakerd Thrust separates the North Makran domain from the Eocene-present day accretionary wedge, which is represented by the Inner, Outer, Coastal, and Off-shore Makran domains (Fig. 1b; Dolati, 2010; Burg et al., 2013; Delavari et al., 2016; Burg, 2018). These domains record the progressive filling of a southward migrating trench and wedge-top basins during the Eocene – Pleistocene (Dolati, 2010; Burg et al., 2013; Burg, 2018).

The BEZO is one of the ophiolite complexes in the western part of North Makran domain (Figs. 1c, Supplementary Figure S1) and represents a MOR-type ophiolite (*sensu* Dilek & Furnes, 2011). It includes, from bottom to top, layered and isotropic gabbros, a sheeted dyke complex, and a volcanic sequence, which is capped by pelagic sedimentary rocks (Supplementary Figure S1; McCall, 1985; Ghazi et al., 2004; Barbero et al., 2020a). ^{40}Ar-^{39}Ar and ^{40}K-^{40}Ar dating on hornblendes from isotropic gabbros (Ghazi et al., 2004) and U/Pb dating on zircons from plagiogranites from the isotropic gabbros (Barbero et al., 2020a; Ghasemi Siani et al., 2021a, b) indicate that the formation of the Band-e-Zeyarat oceanic crust took place during the Early Cretaceous. Geochemical and petrogenetic studies on this ophiolite show that magmatic rocks have both normal (N)- and enriched (E)- mid-ocean ridge basalt (MORB) chemical affinities, with the latter being more abundant with respect to the former (Ghazi et al., 2004; Barbero et al., 2020a). The BEZO together with the ophiolites in the North Makran has been interpreted as the remnants of the oceanic lithosphere of the so-called North Makran Ocean (McCall & Kidd, 1982). A recent study has suggested that the BEZO formed in a mid-ocean ridge that was influenced by embryonic mantle plume magmatism (Barbero et al., 2020a).

The North Makran Ocean has been formerly interpreted either as a back-arc basin formed in response to the subduction of the Neotethyan oceanic lithosphere (McCall & Kidd, 1982; McCall, 1997; Dilek and Furnes, 2019) or as a marginal oceanic basin opened during Late Jurassic – Early Cretaceous times along the southern margin of Eurasia because of rift-related extensional tectonics (Hunziker et al., 2015; Burg, 2018). Regardless of these different interpretations, it was suggested that the opening of this basin led to the rifting of a microcontinental block (the so-called Bajgan-Durkan microcontinent) from the Lut Block (McCall and Kidd, 1982; McCall, 2002; Hunziker et al., 2015; Burg, 2018). However, Barbero et al., (2021a, b, 2023) and Pandolfi et al., (2021) recently demonstrated that the Bajgan and Durkan Complexes represent remnants of Upper Jurassic-Lower Cretaceous meta-ophiolite and tectonically disrupted Late Cretaceous seamount sequences, respectively, rather than the remnants of a microcontinent. The Bajgan Complex consists of meta-gabbros, meta-basalts, and meta-sedimentary rocks derived from high pressure-low temperature metamorphism of MOR-type oceanic lithosphere (Pandolfi et al., 2021). On the contrary, the Durkan Complex includes shallow-water and pelagic meta-sedimentary successions associated with plume-type (P)-MORB and alkaline meta-basalts, recording Late Cretaceous magmatism and sedimentation within a seamount setting (Barbero et al., 2021a, b, 2023).

The structural setting of the BEZO is described by McCall (1985) who recognized that this unit is severely folded and faulted, though he did not describe in detail the deformation history. Nonetheless, the deformation of this ophiolite, along with the whole North Makran Ocean, has been related to the collision-related deformation between the Bajgan-Durkan microcontinent and the southern margin of the Eurasian plate (McCall & Kidd, 1982; McCall, 1997; Hunziker et al., 2015).

Stratigraphy of the crustal section of the Band-e-Zeyarat ophiolite

The BEZO shows a typical upper crustal section of an ophiolite and a sedimentary cover (Supplementary Figure S1; McCall, 1985; Barbero et al., 2020a). The magmatic part is composed of a lower intrusive complex followed by a sheeted dyke complex and a volcanic sequence (Barbero et al., 2020a; Ghasemi Siani et al., 2021a, b). The transition between the magmatic sequence and the sedimentary cover (here named the transition zone) is well exposed to the south of the Kahnuj city (Fig. 2; Supplementary Fig. S1). We studied in detail the Kahnuj area to characterize the stratigraphic architecture of the transition zone and the sedimentary cover and their ages according to the nannofossils contents.

The transition zone sequence

In the area to the south of the Kahnuj city, the transition zone sequence shows lateral variations in thickness, reaching up to hundreds of metres, and is characterized by the alternation of pillow lavas and pillow breccias with lenticular fragments of carbonate rocks (Figs. 2a, 3a, b). Pillow lava flows are decimetres- to metres-thick and lenticular in shape (Figs. 3b, c). Pillow breccias are composed of fragmented pillow lavas and pelagic limestone set in a hyaloclastitic matrix (Fig. 3d). Broken beds of pelagic limestone also occur within the brecciated horizons (Fig. 3e). Sedimentary carbonate rocks within the transition zone reach up to 20 metres in thickness (Figs. 3a, b), and increase upward in the transition zone defining lenticular bodies of pelagic limestone beds embedded within alternating pillow lava and pillow breccia horizons (Figs. 3a, b). These pelagic rocks consist of alternating limestone, cherty limestone, and subordinate marl, with thin- to medium-thick beds, showing clear primary stratigraphic relationships with volcanic rocks (Fig. 3f). These stratigraphic features of the transition zone sequence testify for the interplay between volcanism and pelagic sedimentation during its formation. The transition zone lithological units are crosscut by abundant basaltic dykes, up to a couple of metres thick, that crosscut the bedding planes

in the sedimentary rocks at high angle. The occurrence of these dyke intrusions within the transition zone further indicates that magmatism and pelagic sedimentation were mostly synchronous and developed in tandem.

The sedimentary cover

The sedimentary cover of the BEZO consists mainly of a carbonate sedimentary sequence, whose thickness is ~ 400 – 600 metres (Fig. 4a). To the south of the Kahnuj city, though strongly folded and faulted, detailed stratigraphic observations allow three different members of the sedimentary cover to be distinguished according to their stratigraphic architecture and position (Fig. 4a). These members are, from the lower to the upper stratigraphic position: i) the cherty limestone member; ii) the limestone and marl member; iii) the varicoloured marl member (Fig. 4a). The cherty limestone member consists of up to multi-decimetric beds of micritic and cherty limestone (Fig. 4b), alternating with thin-bedded marl and shale. This member occurs at the base of the sedimentary cover of the BEZO, showing variable thickness (from 10 to 40 metres) and primary stratigraphic relationships with the transition zone (Figs. 3a, 4a). This primary relationship is further demonstrated by the existence of clasts of cherty limestone with soft-sediment deformation within the pillow breccia horizons in the transition zone sequence.

The cherty limestone member passes upward to the limestone and marl member through a gradual stratigraphic transition marked by a significant increase in the thickness of the marly horizons (Fig. 4a). The limestone and marl member is characterized by the alternation of marl, pelagic limestone, and calcareous turbidite (Fig. 4c). In the lower part of this member, the marl horizons are cm to dm in thickness, whereas in the upper part they are up to metres. The calcareous turbidites consist of thin- to medium-thick beds of calcareous turbidites alternating with marl beds. Medium to coarse-grained turbiditic arenitic (in textural meaning) beds are interlayered in the upper part of the limestone and marl member (Figs. 4a, d). These beds define lenticular bodies up to tens

of metres thick and hundreds of metres wide embedded within the alternating marl, limestone, and calcareous turbidite horizons. The petrographic composition of these arenites is characterized by monocrystalline quartz and feldspar and fine-grained lithic fragments (Fig. 4e). Lithic fragments include low to very-low grade metamorphic rocks (phyllite, micaschist and quartzite, Supplementary Figure S2), acidic volcanic rock fragments (mainly rhyolite and dacite), and minor quartz-rich siltstone, fine-grained arenite, and fine-grained carbonate rocks (Supplementary Figure S2). These petrographic observations indicate that the provenance of sediments for these deposits was an exposed metamorphic basement and a volcanic rock terrain.

The varicoloured marl member represents the uppermost part of the sedimentary cover of the BEZO and is unconformably overlain by an Eocene siliciclastic sequence (Fig. 2a). This member consists of alternating pinkish to greyish horizons of marl that are up to metres in thickness (Fig. 4f) and subordinate calcareous turbiditic beds. In addition, thin- to medium-thick beds of fine-grained greyish to brownish turbiditic arenites are interlayered within the varicoloured marl member (Fig. 4a). These beds commonly show an erosive base and are lenticular to tabular in shape (Fig. 4g). They correspond to medium- to coarse-grained volcaniclastic arenites (Fig. 4h); although they are rather altered, their petrographic composition is characterized by plagioclase crystals and intermediate to acidic volcanic or subvolcanic rock-fragments (mainly dacite and andesite). Clasts of brown volcanic glass are quite common showing a complex shape and an early soft-clast deformation (Fig. 4i). In addition, minor lithic fragments of mudstone and minor wackestone with deformed and squeezed soft margins are observed (Supplementary Figure S2). The fine-grained marly part of these turbidites is characterized by the common presence of small fragments of brown volcanic glass (Supplementary Figure S2). The composition of these arenites indicates that volcaniclastic turbiditic material reached the basin during the deposition of the varicoloured marl member.

Biostratigraphy of the transition zone sequence and sedimentary cover

Nannoplankton biostratigraphy has been applied to constrain the depositional age of the sedimentary cover and the transition zone sequence. Fifty-eight samples of marls were collected and prepared as smear-slides for analysis of nannofossils at the Micropaleontology Laboratory of the CNR Institute of Geosciences and Earth Resources following the standard techniques (Bown and Young, 1998). Samples were collected from the transition zone and sedimentary cover sequences of the BEZO. The stratigraphic positions of the representative samples are shown in Figures 3a, 4a. Calcareous nannofossil assemblages have been analysed using a polarising light microscope at 1250× magnification on thirty-five smear-slides as twenty-three samples resulted to be barren. The taxa considered in the nannofossil assemblages are all referenced in Young et al. (2017) and microphotographs of selected taxa are reported in Supplementary Figure S3. Calcareous nannofossil specimens are scarce and poorly preserved. This is because they probably suffered dissolution in a sedimentary setting, which was close to or below the carbonate compensation depth. They also underwent diagenetic recrystallization. The occurrence of the recognized species has been evaluated as the number of specimens observed on a high number of fields of view. Estimations of the nannofossil abundances have been normalized to 1 mm^2 (roughly corresponding to 50 fields of views) and recorded as follow: VR (Very Rare) < 1 specimens/mm^2; R (Rare) 1 - 2 specimens/mm^2; F (Few) 3 - 10 specimens/mm^2; C (Common) >10 specimens/mm^2. Data are reported in Supplementary Table S1, in which the samples are listed following a stratigraphic order. Only a few significant species has been confidently recognized in a few number of samples. Considering the calcareous nannofossil occurrences and their distribution ranges reported in Figure 5, it has been possible to assign broad age ranges, without the possibility to delineate biozonal boundaries, as tighter age constraints.

Two samples taken from a limestone layer embedded in the volcanic sequence and the transition zone sequence (MK5B and MK717, Fig. 3a) contain *Calcicalathina oblongata*

characteristic of the early Valanginian to early Barremian. Without any other reliable data, all these sequences are interpreted as early Valanginian to early Barremian in age. However, indirect constraints on the depositional age of the transition zone sequence can be derived from the age of the overlying cherty limestone member. The lower part of the cherty limestone member (samples MK828 and MK829, Fig. 4a) has been assigned to the early Hauterivian based on the occurrence of *Eprolithus antiquus* that has its first occurrence at the bottom of the Hauterivian. Therefore, integrating stratigraphic and biostratigraphic age data, we assign the age of the transition zone sequence to the Valanginian. The upper part of the cherty limestone member (e.g., sample MK827, Fig. 4a) and the lower part of the limestone and marl member (e.g., sample MK408, Fig. 4a) have been ascribed to the late Hauterivian based on the occurrence of *Lithraphidites bolli,* whose range of total distribution spans the upper part of the Hauterivian. The upper-middle part of the limestone and marl member (e.g., sample MK413, Fig. 4a) has been assigned to the Barremian on the occurrence of *Nannoconus abundans,* which spans this interval of time, and on assemblages that contain *Nannoconus bermudezii* and *Nannoconus steinmanni,* which have their last occurrence in the latest Barremian. Therefore, the cherty limestone member and the limestone and marl member can be ascribed to the early – late Hauterivian and the late Hauterivian – Barremian, respectively. We have not been able to date the varicoloured marl member because the assemblages found in the analysed samples contain few or rare specimens of taxa that are not useful to obtain ages. However, the stratigraphic position above the Barremian limestone and marl member indicates that the varicoloured marl is most likely post-Barremian in age. In addition, foraminifera biostratigraphic investigations performed by McCall (1985) and Samimi Namin (1983) on the same studied sections suggest that the younger part of the sedimentary cover of the BEZO reached the Cenomanian. Therefore, we can reasonably attribute this sequence as post Barremian (?) – Cenomanian (?), though further data are needed to better constrain this age constraint.

Dykes and sills intruding the sedimentary cover

Field relationships between dykes and sills and the sedimentary rocks

A notable feature of the sedimentary cover of the BEZO is the occurrence of basaltic sills and dykes that crosscut the lower and middle parts of the sequence (Fig. 4a). The dykes show various orientations ranging from NW-SE to NE-SW (Fig. 6a). By contrast, the sills represent bedding-parallel (Fig. 2b) tabular intrusive bodies that are preferentially localized within the marl horizons, re-utilizing the limestone-marls stratigraphic interfaces (Fig. 6b). Both the dykes and sills show clear primary intrusive contacts with the sedimentary rocks, as observed by their chilled margins, as well as the recrystallization of the marl layers close to the intrusive contacts (Fig. 6c). The sills are folded by the same deformation phases that affected the sedimentary cover of the BEZO (see following section). This observation indicates the timing of the intrusion of the sills and dykes into the pelagic sequence as a pre-Eocene.

Petrography and geochemistry of dykes and sills in the sedimentary cover

We analysed dykes and sills in the sedimentary cover to characterise their petrographic features and their geochemistry. Petrographic observations indicate that most of the studied samples were affected by variable degrees of secondary alteration resulting in the replacement of their primary magmatic minerals. Plagioclase is commonly replaced by a fine-grained sericite aggregate, whereas clinopyroxene is commonly pseudomorphosed by amphibole or chlorite. Despite this pervasive replacement of the primary mineralogy, magmatic textures of the dyke and sill rocks are still well preserved.

Two different types of textures can be recognized in both dykes and sills. Some samples show a porphyritic texture (PI in the range 15-35) with phenocrysts of euhedral plagioclase set in a groundmass showing intergranular to sub-ophitic textures, whereas other samples show a sub-

ophitic texture. These samples are holocrystalline, inequigranular (from fine- to medium-grained), with euhedral to subhedral plagioclase grains partially included within anhedral clinopyroxene and with Fe-Ti oxides in an interstitial position.

The whole-rock chemical compositions of these rocks were determined by X-ray fluorescence (XRF) and inductively coupled plasma mass spectrometry (ICP-MS). Analytical methods, as well as the accuracy and detection limits are given in Supplementary Text S1. The analytical results are presented in Table 1. Our petrographic study has demonstrated that most of the studied rocks underwent moderate to severe alteration. Large ion lithophile elements (e.g., Ba, Sr, Rb, K) and most major elements are commonly affected by alteration-induced mobilization (Pearce and Norry, 1979). Therefore, the description of the geochemical features of these rocks are based mainly on the contents of those elements, which are considered immobile during low-temperature alteration (Pearce and Norry, 1979). These elements include many incompatible trace elements (e.g., Ti, P, Zr; Y, Sc, Nb, Ta, Hf, Th), rare earth elements (REE), and some transitional metals (e.g., Ni, Co, Cr, V).

Sills and dykes in the sedimentary cover are represented mainly by basalts and one ferro-basalt showing sub-alkaline affinity (Supplementary Figure S4). The Nb/Y ratios are in the range of 0.21 – 0.35 and are comparable with those of E-MORB rocks in the magmatic sequence of the BEZO (Supplementary Figure S4). Mg# values range from 71.8 to 52.7 indicating that these rocks represent melts at different fractionation stage (Table 1). Compatible element abundance is rather low and generally correlates with the Mg#; this is particularly evident for Ni contents that decrease from the most primitive (high Mg#) to the more differentiated (low Mg#) basalts (Table 1). Sill and dyke rocks are characterized by relatively high contents of Nb (5.26-18.6 ppm), Y (21.7-53.6 ppm), Th (0.435-1.92 ppm), Zr (82.1-427 ppm), and Ta (0.37-1.27 ppm). In the N-MORB incompatible element spider diagrams they show enrichment of large ion lithophile elements relative to high field strength elements, displaying decreasing patterns from Th to Y (Fig. 7a). Both slightly positive and negative anomalies in Ti can be observed, likely because of the crystallization or fractionation of

Fe-Ti oxides (Fig. 7a). Chondrite-normalized REE diagram shows decreasing pattern from light (L) REE to heavy (H) REE (Fig. 7b). The overall geochemical features of the sills and dykes in the sedimentary cover suggest an E-MORB chemical affinity that is comparable with the geochemistry of volcanic and subvolcanic rocks observed in the magmatic sequence of the BEZO (Fig. 7). This conclusion is also confirmed by the discrimination diagrams of Figure 7c, d, whereby sill and dyke rocks plot close to the composition of typical E-MORB (Sun & McDonough, 1989). In addition, in the Pearce (2008) diagram, our dyke and sill samples plot along the trend for mantle plume-mid ocean ridge interaction (Fig. 7d). These geochemical characteristics of the dyke and sill rocks collectively suggests that magmatism that produced these intrusions were genetically related to the magmatism that generated the magmatic crust of the BEZO.

Structural setting and deformation history of the Band-e-Zeyarat ophiolite

The BEZO forms a N-S elongated tectonic unit bordered by high angle fault zones and it is unconformably covered by an Eocene sedimentary sequence consisting of conglomerates and arenites (Supplementary Fig. S1). In the western North Makran, the orientation of both the BEZO and the other tectonic units, as well as their tectonic contacts are rotated clockwise with respect to the same structural features in the eastern North Makran (i.e., Fannuj – Maskutan area, Fig. 1c). This rotation was likely the manifestation of right-later faulting along the Minab-Sabzevaran-Nayband fault (e.g., McCall, 1985; Stoneley, 2005). The bedding and the structural elements are hereafter reported in their present-day attitude (i.e., post-rotation orientations, Fig. 2b). At a map scale, the BEZO displays a NNW-striking domal antiformal structure, showing a core composed of lower crustal rocks (mainly gabbros) and sheeted dykes, overlain by the volcanic and transition zone sequences and the sedimentary cover (Supplementary Fig. S1). The domal antiform also deformed the Eocene sequence and its basal unconformity (Supplementary Fig. S1). The limbs of

the domal antiform are commonly deformed by high angle strike-slip faults (Supplementary Fig. S1). Both the domal antiform and the high angle faults deform two generations of folding, namely D1 and D2, which are only recognized in the rocks of the BEZO. The D1 and D2 structures are, in turn, sealed by the Eocene sequence. These structural relationships allow us to demonstrate a relative chronology of the deformation phases observed in the field area; the domal antiform and the high angle faults correspond to a post D1-D2 deformation phase, namely D3 deformation phase, which is recognized in both the BEZO and the Eocene sequence. The D1 and D2 phases are ascribed to pre-Eocene tectonic stages, whereas the D3 phase has been assigned to post-Eocene stages. As already described by McCall (1985), folding related deformation is well recognizable in the BEZO sedimentary cover; by contrast in the other stratigraphic units (i.e., volcanic sequence, sheeted dyke complex, and gabbroic plutons) the mesoscale structures are rarely observed due to the lack of clear stratigraphic markers. For this reason, the structural investigation was carried out by analysing the sedimentary cover in selected areas in the northern part of the field area, near the Kahnuj city, where the Eocene sequence unconformably covers the structures in the BEZO (Figs. 2a, b).

D1 deformation phase

The D1 phase is characterized by recumbent sub-isoclinal to close, similar folds, showing subrounded hinges (Figs. 8a, b). These folds affected both the bedding planes and the sills intruded in the sedimentary cover (Fig. 2b). Thin limestone beds deformed by these folds locally display boudinage structures along the fold limbs and slightly thickened hinge zones (Fig. 8b). The D1 folds are associated with an axial planar foliation S1 (Fig. 8a). S1 is well developed in the marly beds and is oriented at a generally low angle to the bedding (S_0) along the fold limbs (Fig. 8c). In thin section, marl shows evidence for weak pressure solution along the foliation. By contrast, in the more competent limestone beds, S1 foliation is only developed in the hinge zone as a spaced

cleavage showing radial fanning around the hinge (Fig. 8b). In the hinge zone, an intersection lineation between S0 and S1 is locally observed within the marly horizons, corresponding to a pencil cleavage lineation. In the study area, high angle faults border different structural blocks (Fig. 2a); in these blocks, fold axes show different orientations (Fig. 2b). In the western part of the study area and close to the N-S Sabzevaran Fault (Fig. 2a) the axes mainly show a N-S orientation (areas A1, A2; Fig. 2b). By contrast, moving away from the main fault (area A3 see Fig. 2b), the axes show clusters with mainly NE- to NW-SE orientation. The change in orientation of the D1 axes is due to strike-slip faulting along the NNW- to NNE-striking faults (Fig. 2b; see also following section) as well as the slightly non-cylindrical nature of the folds. The asymmetry of D1 folds indicates E- to SW-SSW (Figs. 8b, d) vergence for these folds.

D2 deformation phase

The D2 phase is associated with the formation of open to close folds showing parallel geometry (Fig. 8e). These folds are asymmetric and are characterized by sub-horizontal to gently inclined axial surfaces (Figs. 8e, f). D2 folds are superimposed on the D1 folds and structural elements, showing a Type 3 (*sensu* Ramsay, 1967) interference pattern (Fig. 8g). D2 folds are associated with a weakly developed axial planar cleavage (S2), which is formed in the hinge zones of close folds. This cleavage corresponds to centimetric-spaced anastomosed to planar fracture planes and is sub-horizontal in all the studied areas (Fig. 8h). The fold axes are sub-horizontal to gently plunged and variably oriented. They have N- to NE-trends in the areas close to the Sabzevaran Fault (areas A1, A2; Fig. 2b), whereas far from this fault (area A3 in Fig. 2b) they show a complete distribution from NE-SW to NW-SE orientation. The asymmetry of D2 folds indicates mainly N- to NE vergence, though W-verging folds have been observed close to the Sabzevaran Fault (in the area A1; Fig. 2a). Similar to D1 folds, this variation in the orientation of D2 folds indicates post-D2 strike-slip faulting related deformation (Fig. 2a).

D3 deformation phase

To the south of Kahnuj, the Eocene sedimentary sequence, which unconformably seals the D1 and D2 structures in the pelagic sedimentary cover of the BEZO (Fig. 2a), consists of siliciclastic rocks with alternating arenite, siltstone, and paraconglomerate layers (Fig. 9a). This sequence can be correlated with the Bidak Unit of McCall (1985), dated as early - late Eocene based on Nummulite contents. The arenites are quartz-rich and show abundant lithic fragments of volcanic rocks and limestones. In addition, minor massive lava flows are interbedded in this sequence. The Eocene sequence and the underlying BEZO are deformed by D3 structures represented by the regional-scale NNW-striking antiformal fold (Supplementary Figure S1) that is associated with NNW- to NNE-striking sub-vertical faults showing both right- and left-lateral strike-slip kinematics (Figs. 2a, 9b). These faults define fault-bounded structural blocks (Fig. 2a) where structural elements of D1 and D2 phases show different orientations (see Fig. 2b) due to rotation induced by strike-slip deformation. Close to the mappable faults, the sedimentary cover of the BEZO show open to gentle D3 folds with NNW-trending and sub-vertical axes, as well as with axial planes with NW-SE strike and rather steep dip angles (Figs. 9c, d). They display parallel geometry, and rounded hinges and are locally associated with the development of an axial planar cleavage corresponding to planar fracture planes (Fig. 9c). The character of these folds, their spatial association with main faults, and their axial orientation likely suggest that they represent drag folds formed to accommodate strike-slip movements along NNW-SSE striking faults. Collectively, the NNW- to NNE-directed strike-slip faults and the associated folds accommodate the clockwise rotation of the BEZO with respect to the ophiolites in the eastern North Makran domain (i.e., Fannuj-Maskutan and Remeshk-Mokhtarabad ophiolites, Fig. 1c). This rotation involved the whole North Makran units as indicated by the change in orientation of the structures (folds, thrusts, sheeted dykes

orientation) from E-W to NW-SE and NNW-SSE moving from the eastern to the western North Makran (Fig. 1c, Burg, 2018). In addition, a NE-striking normal fault reworks the stratigraphic contact between the Eocene sequence and the BEZO sedimentary cover in the NE part of the studied area (Fig. 2a).

Discussion

From a mid-oceanic ridge to an accretionary complex: the evolutionary steps of the Band-e-Zeyarat oceanic lithosphere

The published data from Barbero et al (2020a) and the new data presented in this paper allow us to reconstruct the complex tectono-sedimentary evolution of the BEZO in various tectonic settings from its origin to final emplacement. We describe and explain this proposed evolution in three steps below.

Step 1: formation in the mid-ocean ridge setting

The geochemical and petrological data from the magmatic sequence of the BEZO demonstrate that the Neotethyan oceanic crust preserved in it is geochemically composite, showing rocks with both N- and E-MORB affinities (Barbero et al., 2020a). We interpret this oceanic crust to have formed in a mid-ocean ridge setting, which involved a mantle plume–ridge interaction during an embryonic stage of a mantle plume activity in the Early Cretaceous (Fig. 10a; see also Barbero et al., 2020a).

The occurrence and the stratigraphic architecture of a rather thick transition zone between the volcanic and the sedimentary cover sequences indicates synchronous volcanism and pelagic

sedimentation in the basin during the Valanginian – early Hauterivian (Figs. 10a, b). As shown in Figures 3a, b, alternating layers of m-thick carbonate pelagic sequence interbedded within pillow lavas suggest repeated pulses of volcanic activities followed by periods of quiescence characterized by pelagic sedimentation with low depositional rate. The periods of pelagic sedimentation mark the timing of the newly formed oceanic crust shifted away from the main spreading centre and the onset of deposition of cherty limestone. Intrusive and volcanic rocks in the BEZO are characterized by both N- and E-MORB geochemical affinities (Barbero et al., 2020a), whereas the transition zone sequence rocks are composed only of E-MORB affinities. This spatial distribution of the lava flows indicates the eruption of "relatively younger" E-MORB basalts on the seafloor in an off-axis position (Figs. 10a, b). This tectono-sedimentary setting together with the petrogenetic evidence provided by Barbero et al. (2020a) indicate that the BEZO formed in a mid-ocean ridge influenced by the rising of an embryonic mantle plume activity and characterized by rather high spreading rate and off-axis magmatism (Fig. 10a).

The proposed tectono-stratigraphic reconstruction is supported by literature data on modern fast-spreading mid-oceanic ridges (Perfit et al., 1994; Han et al., 2014; Canales et al., 2012). Geophysical investigations have revealed the existence of off-axis magma lenses that can produce magmatism and crustal accretion at wide distance (~ 10-30 km) from the ridge axes (Canales et al., 2012; Han et al., 2014). Furthermore, some differences in the chemical compositions of the lavas erupted along in- and off-axis of these ridges are documented (Perfit et al., 1994; Zou et al., 2002; Turner et al., 2011). These differences are thought to be related to lateral and vertical magma flows, or a different mantle source and melting conditions, or, eventually, a combination of both (Perfit et al., 1994; Zou et al., 2002; Turner et al., 2011).

Step 2: travelling away from the mid-ocean ridge setting

The lower Hauterivian cherty limestone member and the upper Hauterivian – post Barremian limestone and marl member of the sedimentary cover indicate the end of the volcanic activity and the onset of undisturbed pelagic sedimentation in the oceanic basin (Figs. 10a, c). The deposition of these members above the Valanginian transitional zone marked the transition to a homogenous pelagic sedimentation in the basin, suggesting the migration of the preserved oceanic lithosphere away from the MOR setting (Fig. 10b). Basaltic dykes and tabular sills were emplaced in the Hauterivian – Barremian pelagic sedimentary cover when magmatism occured in a within-plate setting far away from the spreading ridge, when the oceanic crust was already covered by a rather thick pelagic sequence (Figs. 10a, c). Our structural analyses indicate that the dykes and sills were deformed by pre-Eocene D1 and D2 deformative phase of the BEZO, ruling out their intrusion in post-Eocene times. Therefore, the crosscutting relationships of these intrusive bodies with the Hauterivian – Barremian sedimentary sequence and our structural data allow us to constrain this magmatic stage as post-Barremian - pre-Eocene.

According to the available data, two hypotheses can be postulated for this post-Barremian - pre-Eocene magmatism (Fig. 10a). The E-MORB geochemical affinity of the subvolcanic rocks of this phase and their similarity with the E-MORB rocks within the magmatic sequence of the BEZO may suggest a genetic relationship between these magmatic events. These geochemical data together with the crosscutting relationships between the subvolcanic bodies and the pelagic sedimentary cover of the BEZO could indicate magmatism associated with a transform fault (hypothesis A in Fig. 10a). In detail, during its drifting away from the axial MOR setting, the Band-e-Zeyarat oceanic lithosphere could have been separated from the ridge by a transform fault (hypothesis A in Fig. 10a). Close to or along the transform fault, off-axis magmatism could involve the migrating oceanic crust already covered by pelagic sedimentation (see grey field as representing the area of intrusion in Fig. 10a, hypothesis A). In this hypothesis, the intrusion of the subvolcanic bodies occurred in a short distance from the ridge, and it is likely very close in time to the formation of the magmatic crust in the ophiolite.

Our second hypothesis envisions that these subvolcanic bodies could be related to within-plate magmatism in response to the migration of the Band-e-Zeyarat oceanic lithosphere above a mantle region with incipient upwelling of deep, hot, and enriched mantle material (Fig. 10a, see hypothesis B). This tectono-magmatic setting can be ascribed to the rising of a mantle plume that is typically characterized by the occurrence of different types of enriched basaltic rocks, ranging from E-MORB to P-MORB and alkaline basalt (Dilek, 2003; Pearce, 2008; Dilek & Furnes, 2011). In addition, the nascent stage of formation of an oceanic island or seamount associated with mantle plume activity is thought to be characterized by tabular sills and dykes intruding the pelagic sedimentary cover of the oceanic crust (Staudigel & Schminke, 1984; Staudigel & Clague, 2010). This phenomenon likely occurred on a wide area of the oceanic basin. Tough the limited extension of the studied area, the stratigraphic and geochemical data suggest that the E-MORB subvolcanic rocks within the sedimentary sequence of the BEZO can be interpreted as volumetrically small remnants of a within-plate magmatic stage associated with the transition of the oceanic lithosphere above a mantle plume (hypothesis B in Fig. 10a). In this scenario, the magmatic phase producing the dykes and sills could have taken place in wide age range, between the formation of the oceanic crust and its accretion into and deformation within the accretionary prism (i.e., between Early Cretaceous and Late Cretaceous).

It is difficult to discriminate between these two hypotheses. However, some pros and cons can be considered for both hypotheses. The chilled margin in the basaltic rocks, the recrystallization of the marls close to the intrusive contact, and the lack of soft-sediment deformation in the marls likely indicate the emplacement of the subvolcanic rocks in an already lithified or nearly lithified Hauterivian – Barremian sedimentary sequence. This evidence suggests that the subvolcanic bodies most likely intruded much later than the formation of the BEZO oceanic lithosphere, supporting the hypothesis B (Fig. 10a). In addition, the comparison with data from other units in the North Makran support that this subvolcanic magmatic stage could be related to an embryonic mantle plume activity. Upper Cretaceous P-MORB and alkaline basalts have been documented from the Durkan

Complex, the Coloured Mélange, the Bajgan Complex, and the Blueschist unit, and they are interpreted as the products of a mature mantle plume activity within the Makran section of Neotethys (Saccani et al., 2018, 2022a, b; Esmaeili et al 2019; Barbero et al., 2021a, b; Pandolfi et al., 2021). Though more data are needed, we favour the hypothesis that this magmatic phase affecting the BEZO and its sedimentary cover occurred during the latest Early Cretaceous time while the oceanic lithosphere was travelling above an embryonic mantle plume (hypothesis B in Fig. 10a).

Step 3: the convergence and deformation within the Makran Accretionary Prism

The occurrence of different types of turbiditic beds within the sedimentary cover of the BEZO testify for the input of siliciclastic sediments in the pelagic basin (Fig. 10c). In particular, the occurrence of turbidites within the upper part of the late Hauterivian – Barremian sedimentary cover (i.e., the limestone and marl member) with lithic fragments of low-grade metamorphic rocks, acidic volcanic rocks, and sedimentary rocks suggest that the turbiditic currents that reached the basin were fed by a neighbouring continental margin domain. Significantly, the occurrence of acidic volcanic rock fragments in the arenites suggests the existence of volcanic arc complex along this margin. In addition, the stratigraphic, biostratigraphic, and petrographic data indicate that volcaniclastic arenite beds are interlayered in the post-Barremian uppermost part of the BEZO sedimentary cover (i.e., the varicoloured marl member). The abundance of volcanic rock clasts in the arenites and their stratigraphic position strongly suggest progressive shifting of the section of the oceanic lithosphere toward an area characterized by the exposure of volcanic rocks during the latest Early Cretaceous (Fig. 10b). The petrographic composition of the volcanic rock fragments with lithic fragments of quartz-rich volcanic rocks and their texture (e.g., occurrence of glass fragments with soft clast deformation and euhedral plagioclase crystals) suggests the exposure in the source area of differentiated volcanic rocks. Collectively, these data on the petrographic

composition of the turbiditic beds and their stratigraphic position indicate that the Band-e-Zeyarat was progressively travelling toward a convergent margin and its trench, whereby a Cretaceous volcanic arc likely existed (Fig. 10a). In the Makran area, remnants of an Early to Late Cretaceous volcanic arc are described within the Coloured Mélange (Saccani et al., 2018) and the Ganj Complex, which was likely built close or onto the Lut continental margin (Barbero et al., 2020b). In addition, evidence for Cretaceous volcanic arcs is also provided by Mohammadi et al. (2016, 2017) based on provenance analysis and detrital zircon geochronology and isotope composition carried out on Upper Cretaceous – Miocene turbidites from the onshore Makran Accretionary Prism. Therefore, our new data combined with literature data indicate travelling of the Band-e-Zeyarat oceanic lithosphere toward the latest Early Cretaceous Makran convergent margin (Fig. 10a).

The deformation history recognized in the BEZO allow us to discuss how this ophiolite has been deformed during the convergence stages. In contrast to what has been previously proposed by McCall and Kidd (1982), the lack of a metamorphic sole at the base of the BEZO allows us to exclude obduction processes as the mechanism of deformation. In addition, recent data on the Bajgan and Durkan Complexes (Barbero et al., 2021a, b, 2023; Pandolfi et al., 2021) indicate that the oceanic lithosphere now preserved in most of the North Makran units was accreted in a Late Cretaceous – early Paleocene subduction complex via underplating at depths typical of HP-LT metamorphism. In the subduction complexes, the transfer of slices from the lower plate to the accretionary prism occurs either at the front of the prism by offscraping (e.g., Kusky and Bradley, 1999; Festa et al., 2013) or at its base by underplating (e.g., Sample and Fisher, 1986; Kimura and Mukai, 1991; Marroni et al., 2004; Meneghini et al., 2009). The offscraping is generally characterized by the accretion of pelagic deposits that display pervasive soft-sediment deformations achieved during their transfer at the toe of the prism (e.g., Festa et al., 2013). In contrast, the underplating consists of the transfer of both magmatic and sedimentary sequences at the base of the prism. The underplating may occur by transfer of slices with a mélange fabric (i.e., the diffusive underplating; Festa et al., 2022), or by the accretion of large bodies that, even if characterized by

internal folding, largely preserve their stratigraphy (i.e., the coherent underplating; Marroni et al., 2004). In the BEZO, the lack of soft sediment deformation and mélange bodies, the preservation of the stratigraphy, and the pervasive folding in the sedimentary deposits indicate that the BEZO was accreted by coherent underplating within the Makran Accretionary Prism (Fig. 10a). The feature of S1 foliation without any metamorphic recrystallization, constrains the underplating of the oceanic lithosphere at shallow structural levels (Fig. 10a). After a simple retro-deformation (i.e., a counter-clockwise rotation) of strike-slip faulting induced deformation, the vergence of the macro-structures of the D1 phase can be reconstructed as to the south to south-east. These interpretations agree with structural analyses in the eastern Makran (i.e., Fannuj area, see Fig. 1c), where the direction of emplacement of various tectonic units was established as toward the south (Dolati, 2010; Dolati & Burg, 2013; Hunziker, 2014; Burg et al., 2013). The greater dispersion of the fold axis detected in the studied area is likely related to strike-slip deformation during the post-Eocene phase. The D1 structural elements are folded by D2 open to close folds, which show a weakly developed and spaced S2 cleavage as axial plane. These overprinting relationships between D1 and D2 phases likely record the progressive exhumation of the BEZO (Fig. 10a) in agreement with data from many accretionary prisms where exhumation was progressively achieved through sub-horizontal folding acting in equilibrating the overgrowth of the frontal prism (Davis et al., 1983; Platt, 1986, 1993; Marroni et al., 2004; Di Rosa et al., 2017; Sanità et al., 2021). The unconformable deposition of the Eocene siliciclastic deposits on top of the structures formed during both D1 and D2 phases further marks the final exhumation of the BEZO. The Early Cretaceous age of the pelagic sedimentary cover sequence together with the Eocene age of the unconformably overlying siliciclastic sequence (see McCall, 1985; Samini Namin, 1983) suggest that the oceanic lithosphere was deformed between the Late Cretaceous and the Paleocene (Fig. 10a). These ages represent a minimum age of these deformation phase. A Maastrichtian unconformity has been observed above the ophiolites in the eastern North Makran possibly suggesting a major upheaval during the latest Late Cretaceous (Dolati, 2010; Burg, 2018). Finally, the features of the D3 deformation phase indicate a strike-slip

deformation of the accreted oceanic material and the Eocene siliciclastic sequence. This phase resulted in the reorientation of structural elements of the D1 and D2 phases as indicated by significant variations in their orientations (Fig. 2b). Mesoscale data and the comparison with structural data from the eastern North Makran suggest that D3 phase was possibly associated with the reactivation of the right-lateral Minab-Sabzevaran fault system during the late Miocene – Pliocene (Stoneley, 2005; Regard et al., 2010). This reactivation likely induced the clockwise rotation of the previously formed accretionary prism structures. This fault system accommodated for different deformation styles in the Zagros and Makran accretionary prisms that are characterized by continent-continent collision and still active subduction zone processes, respectively. Further biostratigraphic and structural data on the post-Eocene sedimentary sequence would be very useful to better constrain the age and regional-scale significance of the D3 phase.

Conclusions

The Band-e-Zeyarat ophiolite (BEZO) includes Early Cretaceous oceanic lithosphere and its sedimentary cover that have been incorporated into the Makran Accretionary Prism. This study documents the tectono-sedimentary evolution of the pelagic sedimentary cover through a multidisciplinary study integrating stratigraphic-biostratigraphic, structural, arenite petrography, and whole rock geochemical data from dykes and sills intruded into the pelagic sequence. The conclusions of this work are summarized as follows:

1) The BEZO includes a transition zone recording a stratigraphic passage from the volcanic sequence to the pelagic sedimentary cover of the ophiolite. The transition zone rocks are Valanginian in age and record the interplay of volcanism and pelagic sedimentation, which took place in a mid-ocean ridge environment and off mid-ocean ridge and within-plate settings.

2) The sedimentary cover consists of a pelagic sequence showing three superimposed members: the basal cherty limestone member (lower Hauterivian), the upper Hauterivian – Barremian limestone and marl member, as well as the Barremian – Cenomanian (?) varicoloured marl member. This upward fining sedimentary sequence points to the stabilization of the depositional setting in an abyssal environment.
3) Dyke and sill intrusions with an E-MORB geochemical affinity within the cherty limestone and limestone and marl members of the sedimentary cover are likely the manifestations of within-plate magmatism associated with an embryonic mantle plume.
4) The intercalations of turbiditic arenites within the limestone and marl and varicoloured marl members in the sedimentary cover indicate proximal location of the BEZO oceanic lithosphere to a convergent margin, where siliciclastic debris from quartz-rich volcanic arc rocks and continental margin basement fed the depositional basin.
5) The BEZO oceanic lithosphere and its sedimentary cover were deformed during their initial underplating beneath the accretionary prism and then during their exhumation in the North Makran prism. The accretionary prism was subsequently deformed by late Miocene - Pliocene strike-slip faulting, which was associated with the re-activation of the Minab-Sabzevaran fault system.

Acknowledgments

The research has been funded by Darius Project (Head M. Marroni), PRA project of the Pisa University (Head S. Rocchi), IGG-CNR, FAR-2022 Project of the Ferrara University (Head E. Saccani). Mr. Ahmad Behboodi is warmly thanked for his fundamental assistance in organizing field work. PhD student Ahmad Nateghpour from Kharazmi University is acknowledged for his kind and fundamental help during field work. We would like to express our gratitude to two

anonymous reviewer and to G. Nirta for their thorough reviews from which we have greatly benefited in revising our paper. Y. Dilek is warmly acknowledged for his careful editorial handling, his insightful comments and reviews of an earlier version, and extensive editing of a revised version of this manuscript.

References

Barbero, E. 2021. *Geological and petrological investigation of the western North Makran ophiolites (SE Iran): new constraints for the Late Jurassic-Cretaceous tectono-magmatic and geodynamic evolution of the Neo-Tethys Ocean*. PhD Thesis, University of Ferrara, Italy, p. 324.

Barbero, E., Delavari, M., Dolati, A., Vahedi, L., Langone, A., Marroni, M., Pandolfi, L., Zaccarini, F. and Saccani, E. 2020a. Early Cretaceous Plume–Ridge Interaction Recorded in the Band-e-Zeyarat Ophiolite (North Makran, Iran): New Constraints from Petrological, Mineral Chemistry, and Geochronological Data. *Minerals*, **10**, 1100, doi:10.3390/min10121100.

Barbero, E., Delavari, M., Dolati, A., Saccani, E., Marroni, M., Catanzariti, R. and Pandolfi, L. 2020b. The Ganj Complex reinterpreted as a Late Cretaceous volcanic arc: Implications for the geodynamic evolution of the North Makran domain (southeast Iran). *Journal of Asian Earth Science*, https://doi.org/10.1016/j.jseaes.2020.104306.

Barbero, E., Pandolfi, L., Delavari, M., Dolati, A., Saccani, E., Catanzariti, R., Luciani, V., Chiari, M. and Marroni, M. 2021a. The western Durkan Complex (Makran Accretionary Prism, SE Iran): A Late Cretaceous tectonically disrupted seamounts chain and its role in controlling deformation style. *Geoscience Frontiers*, **12**, https://doi.org/10.1016/j.gsf.2020.12.001.

Barbero, E., Zaccarini, F., Delavari, M., Dolati, A., Saccani, E., Marroni, M. and Pandolfi, L. 2021b. New evidence for Late Cretaceous plume-related seamounts in the Middle East sector of the Neo-Tethys: Constraints from geochemistry, petrology, and mineral chemistry of the magmatic

rocks from the western Durkan Complex (Makran Accretionary Prism, SE Iran). *Lithos*, 396–397, 106228. https://doi.org/10.1016/j.lithos.2021.106228

Barbero, E., Di Rosa, M., Pandolfi, L., Delavari, M., Dolati, A., Zaccarini, F., Saccani, E. and Marroni, M. 2023. Deformation history and processes during accretion of seamounts in subduction zones: The example of the Durkan Complex (Makran, SE Iran). *Geoscience Frontiers*, **14**, 101522. https://doi.org/10.1016/j.gsf.2022.101522

Barrier, E., Vrielynck, B., Brouillet, J.F. and Brunet, M.F. 2018. Paleotectonic Reconstruction of the Central Tethyan Realm. Tectono-Sedimentary-Palinspastic maps from Late Permian to Pliocene. Atlas of 20 maps (scale: 1:15.000.000). CCGM/CGMW, Paris, http://www.ccgm.org.

Bown P.R. and Young J.R. 1998. Techniques. *In*: Bown, P.R. (Ed.), *Calcareous Nannofossil Biostratigraphy. British Micropalaeontology Society Publication Series*. Kluwer Academic Publishers, Dordrecht, pp. 16–28.

Burg, J.-P. 2018. Geology of the onshore Makran accretionary wedge: Synthesis and tectonic interpretation. *Earth-Science Reviews*, **185**, 1210-1231. https://doi.org/10.1016/j.earscirev.2018.09.011.

Burg, J.-P., Dolati, A., Bernoulli, D. and Smit, J. 2013. Structural style of the Makran tertiary accretionary complex in SE Iran. *In*: Al Hosani, K., Roure, F., Ellison, R., Lokier, S. (Eds.), *Lithosphere Dynamics and Sedimentary Basins: The Arabian Plate and Analogues*. Frontiers in Earth Sciences, Springer, Heidelberg, pp. 239-259. https://doi.org/10.1007/978-3-642-30609-9_12

Canales, J. P., Carton, H., Carbotte, S. M., Mutter, J. C., Nedimović, M. R., Xu, M., Aghaei, O., Marjanović, M. and Newman, K. 2012. Network of off-axis melt bodies at the East Pacific Rise. *Nature Geoscience*, **5(4)**, 279–283. https://doi.org/10.1038/ngeo1377

Davis, D., Suppe, J. and Dahlen, F. A. 1983. Mechanics of fold-and-thrust belts and accretionary wedges. *Journal of Geophysical Research*, **88(B2)**, 1153–1172.

Delavari, M., Dolati, A., Marroni, M., Pandolfi, L. and Saccani, E. 2016. Association of MORB and SSZ ophiolites along the shear zone between coloured Melange and Bajgan complexes (North

Makran, Iran): Evidence from the Sorkhband area. *Ofioliti*, **41(1)**, 21–34. https://doi.org/10.4454/ofioliti.v41i1.440

Dercourt, J., Zonenshian, L.P., Ricou, L.E., Kazmin, V.G., LePichon, X., Knipper, A.L., Grandjacquet, C., Sbortshikov, M., Geyssant, J., Lepvrier, C., Pechersky, D.H., Boulin, J., Sibuet, J.C., Savostin, L.A., Sorokhtin, O., Westphal, M., Bazhenov, M.L., Lauer, J.P. and Biju-Duval, B. 1986. Geological evolution of the Tethys Belt from the Atlantic to the Pamir since the Lias. *Tectonophysics*, **123**, 241-315.

Dewey, J.F. and Bird, J.M. 1971, The origin and emplacement of the ophiolite suite: Appalachian ophiolites in Newfoundland. *Journal of Geophysical Research*, **76**, 3179–3206, doi: 10.1029/JB076i014p03179.

Dilek, Y., 2003. Ophiolites, plumes and orogeny: *In:* Dilek, Y. and Robinson, P.T. (eds.), *Ophiolites in Earth History*. Geological Society of London Special Publication, v. 218, p. 9-19.

Dilek, Y. and Furnes, H. 2014. Ophiolites and Their Origins. *Elements*, **10(2)**, 93–100. https://doi.org/10.2113/gselements.10.2.93

Dilek, Y. and Furnes, H. 2011. Ophiolite genesis and global tectonics: geochemical and tectonic fingerprinting of ancient oceanic lithosphere. *Geological Society of America Bulletin*, **123**, 387-411.

Dilek, Y. and Furnes, H. 2019. Tethyan ophiolites and Tethyan seaways. *Journal of the Geological Society of London*, **176(5)**, 899-912, doi: 10.1144/jgs2019-129

Di Rosa, M., De Giorgi, A., Marroni, M. and Pandolfi, L. 2017. Geology of the area between golo and tavignano valleys (central corsica): A snapshot of the continental metamorphic units of alpine corsica. *Journal of Maps*, **13(2)**, 644–653. https://doi.org/10.1080/17445647.2017.1351900

Dolati, A. 2010. *Stratigraphy, Structure Geology and Low-temperature Thermochronology Across the Makran Accretionary Wedge in Iran*. PhD thesis, ETH Zurich, 165 pp.

Dolati, A. and Burg, J.-P. 2013. Preliminary fault analysis and paleostress evolution in the Makran Fold-and-Thrust Belt in Iran. *In*: Al Hosani, K., Roure, F., Ellison, R., Lokier, S. (Eds.),

Lithosphere Dynamics and Sedimentary Basins: The Arabian Plate and Analogues. Frontiers in Earth Sciences, Springer, Heidelberg, pp. 261–277. https://doi.org/10.1007/978-3-642-30609-9_13

Eftekhar-Nezhad, J., Arshadi, S., Mahdavi, M.A., Morgan, K.H., McCall, G.J.H. and Huber, H. 1979. *Fannuj Quadrangle Map 1:250000*. Ministry of Mines and Metal, Geological Survey of Iran, Tehran.

Esmaeili, R., Xiao, W., Ebrahimi, M., Zhang, J., Zhang, Z., Abd El-Rahman, Y., Han, C., Wan, B., Ao, S., Song, D., Shahabi, S. and Aouizerat, A. 2019. Makran ophiolitic basalts (SE Iran) record Late Cretaceous Neotethys plume-ridge interaction. *International Geology Review*, 1–21. https://doi.org/10.1080/00206814.2019.1658232

Esmaeili, R., Xiao, W., Griffin, W. L., Moghadam, H. S., Zhang, Z., Ebrahimi, M., Zhang, J., Wan, B., Ao, S. and Bhandari, S. 2020. Reconstructing the Source and Growth of the Makran Accretionary Complex: Constraints From Detrital Zircon U-Pb Geochronology. *Tectonics*, **39(2)**. https://doi.org/10.1029/2019TC005963

Festa, A., Dilek, Y., Mittempergher, S., Ogata, K., Pini, G. A. and Remitti, F. 2018. Does subduction of mass transport deposits (MTDs) control seismic behavior of shallow–level megathrusts at convergent margins?. *Gondwana Research*, **60**, 186–193. https://doi.org/10.1016/j.gr.2018.05.002

Festa, A., Dilek, Y., Codegone, G., Cavagna, S. and Pini, G.A. 2013. Structural anatomy of the Ligurian accretionary wedge (Monferrato, NW Italy), and evolution of superposed mélanges. *Geological Society of America Bulletin*, **125**, 1580–1598, https://doi.org/10.1130/B30847.1

Festa, A., Barbero, E., Remitti, F., Ogata, K. and Pini, G.A. 2022. Mélanges and chaotic rock units: Implications for exhumed subduction complexes and orogenic belts. *Geosystems and Geoenvironment*, **1(2)**, 100030, https://doi.org/10.1016/j.geogeo.2022.100030.

Furnes, H., Dilek, Y., Zhao, G.-C., Safonova, I. and Santosh, M., 2020. Geochemical characterization of ophiolites in the Alpine-Himalayan orogenic belt: Magmatically & tectonically diverse evolution of the Mesozoic Neotethyan oceanic crust. *Earth-Science Reviews*, **208**, 103258.

Furnes, H. and Dilek, Y., 2021. Archean versus Phanerozoic oceanic crust formation and tectonics: Ophiolites through time. *Geosystems and Geoenvironment*, **1(1)**, https://doi.org/10.1016/j.geogeo.2021.09.004.

Ghasemi Siani, M., Mehrabi, B., Neubauer, F. and Cao, S. 2021a. Trace element geochemistry of zircons from the Kahnouj ophiolite complex: implications for petrogenesis and geodynamic setting. *Arabian Journal of Geosciences*, **14(14)**, 1377. https://doi.org/10.1007/s12517-021-07575-5

Ghasemi Siani, M., Mehrabi, B., Neubauer, F., Cao, S. and Lentz D.R. 2021b. Geochronology, geochemistry, and origin of plagiogranitic rocks and related granitic dikes in the Dar Gaz district, Kahnouj ophiolite complex, SE Iran: Analysis of their petrogenesis in a back-arc tectonic setting. *Lithos*, **380-381**, 105832, https://doi.org/10.1016/j.lithos.2020.105832

Ghazi, A.M., Hassanipak, A.A., Mahoney, J.J. and Duncon, R.A. 2004. Geochemical characteristics, 40Ar-39Ar ages and original tectonic setting of the Band-e-Zeyarat/Dar Anar ophiolite, Makran accretionary Prism, S.E. Iran. *Tectonophysics*, **193**, 175-196. 10.1144/GSL.SP.1984.016.01.02

Glennie, K.W., Hughes Clarke, M.W., Boeuf, M.G.A., Pilaar, W.F.H. and Reinhardt, B.M. 1990. Inter-relationship of Makran-Oman Mountains belts of convergence. *Geological Society of London Special Publications*, **49**, 773–786. https://doi.org/10.1144/GSL.SP.1992.049.01.47

Gradstein F.M., Ogg J.G., Schmitz M.D. and Ogg G.M. 2012. The geologic time scale 2012. *Elsevier Publication*, Amsterdam, pp 85–114.

Han, S., Carbotte, S. M., Carton, H., Mutter, J. C., Aghaei, O., Nedimović, M. R. and Canales, J. P. 2014. Architecture of on- and off-axis magma bodies at EPR 9°37–40′N and implications for oceanic crustal accretion. *Earth and Planetary Science Letters*, **390**, 31–44. https://doi.org/10.1016/j.epsl.2013.12.040

Hanan, B. B., Blichert-Toft, J., Kingsley, R. and Schilling, J.-G. 2000. Depleted Iceland mantle plume geochemical signature: Artifact of multicomponent mixing? *Geochemistry, Geophysics, Geosystems*, **1**. https://doi.org/10.1029/1999GC000009

Hunziker, D. 2014. *Magmatic and metamorphic history of the North Makran ophiolites and blueschists (SE Iran): Influence of Fe3+/Fe2+ ratios in blueschist facies minerals on geothermobarometric calculations*. PhD Thesis, ETH Zurich, Switzerland, 364 pp.

Hunziker, D., Burg, J.-P., Bouilhol, P. and von Quadt, A. 2015. Jurassic rifting at the Eurasian Tethys margin: Geochemical and geochronological constraints from granitoids of North Makran, southeastern Iran. *Tectonics*, **34**, 571-593. 10.1002/2014TC003768

Hunziker, D., Burg, J.-P., Moulas, E., Reusser, E. and Omrani, J. 2017. Formation and preservation of fresh lawsonite: Geothermobarometry of the North Makran Blueschists, southeast Iran. *Journal of Metamorphic Geology*, **35(8)**, 871–895. https://doi.org/10.1111/jmg.12259

Isozaki, Y., Maruyama, S. and Furuoka, F. 1990. Accreted oceanic materials in Japan. *Tectonophysics*, **181**, 179–205. https://doi.org/10.1016/0040-1951(90)90016-2

Kananian, A., Juteau, T., Bellon, H., Darvishzadeh, A., Sabzehi, M., Whitechurch, H. and Ricou, L.-E. 2001. The ophiolite massif of Kahnuj (western Makran, southern Iran): new geological and geochronological data. *C. R. Acad. Sci. Ser. IIA Earth Planet. Sci.*, **332**, 543–552.

Khalili, M., Dilek, Y., and Ronizi, L.Z. 2022. Quaternary deformation patterns in east–central Iran, constrained by coseismic–postseismic displacements of the 2017 Hojedk triplet earthquake in the Kerman Province. *Journal of Geodynamics*, https://doi.org/10.1016/ j.jog.2022.101941.

Kimura, G. and Mukai, A. 1991. Underplated units in an accretionary complex: Melange of the Shimanto Belt of eastern Shikoku, southwest Japan. *Tectonics*, **10(1)**, 31–50. https://doi.org/10.1029/90TC00799

Kusky, T. M. and Bradley, D. C. 1999. Kinematic analysis of mélange fabrics: examples and applications from the McHugh Complex, Kenai Peninsula, Alaska. *Journal of Structural Geology*, **21(12)**, 1773–1796. https://doi.org/10.1016/S0191-8141(99)00105-4

Kusky, T.M., Windley, B.F., Safonova, I., Wakita, K., Wakabayashi, J., Polat, A. and Santosh, M. 2013. Recognition of ocean plate stratigraphy in accretionary orogens through Earth history: A

record of 3.8 billion years of sea floor spreading, subduction, and accretion. *Gondwana Research*, **24**, 501–547. https://doi.org/10.1016/j.gr.2013.01.004

Marroni, M., Meneghini, F. and Pandolfi, L. 2004. From accretion to exhumation in a fossil accretionary wedge: a case history from Gottero unit (Northern Apennines, Italy). *Geodinamica Acta*, **17(1)**, 41–53. https://doi.org/10.3166/ga.17.41-53

Meneghini, F., Marroni, M., Moore, J.C., Pandolfi, L. and Rowe, C.D. 2009. The record of underthrusting and underplating in the geologic record: Structural diversity between the Franciscan Complex (California), the Kodiak Complex (Alaska) and the Internal Ligurian Units (Italy). *Geological Journal*, **44**, 126–152, https://doi.org/10.1002/gj.1144

McCall, G.J.H. 1985. Explanatory text of the Minab Quadrangle Map; 1:250,000; No. J13. Geological Survey of Iran, Tehran, pp. 530.

McCall, G.J.H. 1997. The geotectonic history of the Makran and adjacent areas of southern Iran. *Journal of Asian Earth Sciences*, **15**, 517-531

McCall, G.J.H. 2002. A summary of the geology of the Iranian Makran. *In*: Clift, P.D., Kroon, F.D., Gaedecke, C., Craig, J. (Eds.), *The Tectonic and Climatic Evolution of the Arabian Sea Region*, Geological Society of London Special Publications vol. 195, pp. 147-204.

McCall, G.J.H. and Kidd, R.G,W. 1982. The Makran southeastern Iran: the anatomy of a convergent margin active from Cretaceous to present. *In*: Leggett, J.K. (Ed.), *Trench-forearc geology: sedimentation and tectonics of modern and ancient plate margins*, Geological Society of London Special Publications vol. 10, pp. 387-397.

Moghadam, H. S., Arai, S., Griffin, W. L., Khedr, M. Z., Saccani, E., Henry, H., O'Reilly, S. Y. and Ghorbani, G. 2022. Geochemical variability among stratiform chromitites and ultramafic rocks from Western Makran, South Iran. *Lithos*, **412–413**, 106591. https://doi.org/10.1016/j.lithos.2021.106591

Mohammadi, A., Burg, J.-P., Winkler, W., Ruh, J. and von Quadt, A. 2016. Detrital zircon and provenance analysis of Late Cretaceous–Miocene onshore Iranian Makran strata: Implications for

the tectonic setting. *Geological Society of America Bulletin*, **128**, 1481–1499. https://doi.org/10.1130/B31361.1

Mohammadi, A., Burg, J.-P., Guillong, M. and von Quadt, A. 2017. Arc magmatism witnessed by detrital zircon U-Pb geochronology, Hf isotopes and provenance analysis of Late Cretaceous-Miocene sandstones of onshore western Makran (SE Iran). *American Journal of Science*, **317(8)**, 941–964. https://doi.org/10.2475/08.2017.03

Pandolfi, L., Barbero, E., Marroni, M., Delavari, M., Dolati, A., Di Rosa, M., Frassi, C., Langone, A., Farina, F., MacDonald, C. S. and Saccani, E. 2021. The Bajgan Complex revealed as a Cretaceous ophiolite-bearing subduction complex: A key to unravel the geodynamics of Makran (southeast Iran). *Journal of Asian Earth Sciences*, **222**, 104965. https://doi.org/10.1016/j.jseaes.2021.104965

Pearce, J. A. 2008. Geochemical fingerprinting of oceanic basalts with applications to ophiolite classification and the search for Archean oceanic crust. *Lithos*, **100(1–4)**, 14–48. https://doi.org/10.1016/j.lithos.2007.06.016

Pearce, J. A. 2014. Immobile Element Fingerprinting of Ophiolites. *Elements*, **10(2)**, 101–108. https://doi.org/10.2113/gselements.10.2.101

Pearce, J.A. and Norry, M.J. 1979. Petrogenetic implications of Ti, Zr, Y, and Nb variations in volcanic rocks. *Contributions to Mineralogy and Petrology*, **69**, 33-47.

Perfit, M. R., Fornari, D. J., Smith, M. C., Bender, J. F., Langmuir, C. H. and Haymon, R. M. 1994. Small-scale spatial and temporal variations in mid-ocean ridge crest magmatic processes. *Geology*, **22(4)**, 375–379. https://doi.org/10.1130/0091-7613(1994)022<0375:SSSATV>2.3.CO;2

Platt, J. P. 1986. Dynamics of orogenic wedges and the uplift of high-pressure metamorphic rocks. *Geological Society of America Bulletin*, **97(9)**, 1037-1053. https://doi.org/10.1130/0016-7606(1986)97<1037:DOOWAT>2.0.CO;2

Platt, J.P. 1993. Exhumation of high-pressure rocks: a review of concepts and processes. *Terra Nova*, **5**, 119-133.

Ramsay, J.G. 1967. Folding and Fracturing of Rocks. Mc Graw and Hill ed. (568 p.).

Regard, V., Hatzfeld, D., Molinaro, M., Aubourg, C., Bayer, R., Bellier, O., Yamini-Fard, F., Peyret, M. and Abbassi, M. 2010. The transition between Makran subduction and the Zagros collision: recent advances in its structure and active deformation. *Geological Society London Special Publications*, **330(1)**, 43–64. https://doi.org/10.1144/SP330.4

Saccani, E. 2015. A new method of discriminating different types of post-Archean ophiolitic basalts and their tectonic significance using Th-Nb and Ce-Dy-Yb systematics. *Geoscience Frontiers*, **6**, 481-501.

Saccani, E., Delavari, M., Dolati, A., Marroni, M., Pandolfi, L., Chiari, M. and Barbero, E. 2018. New insights into the geodynamics of Neo-Tethys in the Makran area: Evidence from age and petrology of ophiolites from the Coloured Mélange Complex (SE Iran). *Gondwana Research*, **62**, 306-327.

Saccani, E., Dilek, Y., Marroni, M. and Pandolfi, L. 2015. Continental margin ophiolites of Neotethys: Remnants of Ancient Ocean–Continent Transition Zone (OCTZ) lithosphere and their geochemistry, mantle sources and melt evolution patterns. *Episodes*, **38(4)**, 230–249. https://doi.org/10.18814/epiiugs/2015/v38i4/82418

Saccani, E., Delavari, M., Dolati, A., Pandolfi, L., Barbero, E., Tassinari, R. and Marroni, M. 2022a. Geochemistry of basaltic blueschists from the Deyader Metamorphic Complex (Makran Accretionary Prism, SE Iran): New constraints for magma generation in the Makran sector of the Neo-Tethys. *Journal of Asian Earth Sciences*, **228**, 105141. https://doi.org/10.1016/j.jseaes.2022.105141

Saccani, E., Delavari, M., Dolati, A., Pandolfi, L., Barbero, E., Brombin, V. and Marroni, M. 2022b. Geochemistry of volcanic rocks and dykes from the Remeshk-Mokhtarabad and Fannuj-Maskutan Ophiolites (Makran Accretionary Prism, SE Iran): New constraints for magma generation in the Middle East Neo-Tethys. *Geosystems and Geoenvironment*, 100140. https://doi.org/10.1016/j.geogeo.2022.100140

Samimi Namin, M. 1982. *Geological Map of Taherui 1:250000 Scale*. Tehran: Ministry of Mines and Metal, Geological Survey of Iran.

Samimi Namin, M. 1983. *Geological Map of Minab 1:250000 Scale*. Tehran: Ministry of Mines and Metal, Geological Survey of Iran.

Sample, J.C. and Fisher, D.M. 1986. Duplex accretion and underplating in an ancient accretionary complex, Kodiak Islands, Alaska. *Geology*, **14**, 160–163.

Sanità, E., Lardeaux, J. M., Marroni, M., Gosso, G. and Pandolfi, L. 2021. Structural relationships between Helminthoid Flysch and Briançonnais Units in the Marguareis Massif: A key for deciphering the finite strain pattern in the external southwestern Alps. *Geological Journal*, **56(4)**, 2024–2040. https://doi.org/10.1002/gj.4040

Sepidbar, F., Lucci, F., Biabangard, H., Zaki Khedr, M. and Jiantang, P. 2020. Geochemistry and tectonic significance of the Fannuj-Maskutan SSZ-type ophiolite (Inner Makran, SE Iran). *International Geology Review*, https://doi.org/10.1080/00206814.2020.1753118

Shervais, J. W. 2001. Birth, death, and resurrection: The life cycle of suprasubduction zone ophiolites. *Geochemistry, Geophysics, Geosystems*, **2(1)**, n/a-n/a. https://doi.org/10.1029/2000GC000080

Sissingh, W. 1977. Biostratigraphy of Cretaceous calcareous nannoplankton. *Geol. Mijnb.*, **56**, 37-65

Staudigel, H. and Clague, D.A. 2010. The geological history of deep-sea volcanoes: Biosphere, hydrosphere, and lithosphere interactions. *Oceanography*, **23**, 58–71. https://doi.org/10.2307/24861062

Staudigel, H. and Schmincke, H.-U. 1984. The Pliocene seamount series of La Palma/Canary Islands. *Journal of Geophysical Research Solid-Earth*, **89(B13)**, 11195–11215. https://doi.org/10.1029/JB089iB13p11195

Stoneley, R. 2005. The Zendan Fault of southern Iran. *Proceedings of the Geologists' Association*, **116(3–4)**, 311–313. https://doi.org/10.1016/S0016-7878(05)80049-5

Sun, S.S. and McDonough, W.F. 1989. Chemical and isotopic systematics of oceanic basalts: implications for mantle composition and processes. *In*: Saunders, A.D., Norry, M.J. (Eds.), *Magmatism in the Ocean Basins*. Geological Society of London Special Publication 42, 313-345.

Turner, S., Beier, C., Niu, Y. and Cook, C. 2011. U-Th-Ra disequilibria and the extent of off-axis volcanism across the East Pacific Rise at 9°30′N, 10°30′N, and 11°20′N. *Geochemistry, Geophysics, Geosystems*, **12(7)**, n/a-n/a. https://doi.org/10.1029/2010GC003403

Wakita, K. 2015. OPS mélange: a new term for mélanges of convergent margins of the world. *International Geology Review*, **57(5–8)**, 529–539. https://doi.org/10.1080/00206814.2014.949312

Young, J.R., Bown, P.R. and Lees, J.A. 2017. Nannotax3 website. *International Nannoplankton Association*. Accessed 21 Apr. 2017. URL: http://www.mikrotax.org/Nannotax3.

Zou, H., Zindler A. and Niu, Y. 2002. Constraints on Melt Movement Beneath the East Pacific Rise From 230Th-238U Disequilibrium. *Science*, **295(5552)**, 107–110. https://doi.org/10.1126/science.1064295

Tables captions

Table 1: Major (wt%) and trace (ppm) element composition of representative subvolcanic rocks from the pelagic sedimentary cover of the Band-e-Zeyarat ophiolite. Abbreviations: XRF: X-ray fluorescence spectrometry; ICP-MS: inductively coupled plasma-mass spectrometry; Mg# = molar proportion of 100 x MgO / (MgO + FeO). Fe2O3=0.15 x FeO. Normalizing values for $(La/Yb)_N$, and $(Sm/Yb)_N$, are from Sun and McDonough (1989).

Figures caption

Figure 1: Maps and cross section of the Makran Subduction accretionary Complex. (a) Location of the Makran Accretionary Prism and main tectonic plates in the Alpine-Himalayan belt (modified from Festa et al., 2018). (b) Sketch of the tectono-stratigraphic elements of the Makran Accretionary Prism drawn above a grey-shaded relief map (from http://www.ngdc.noaa.gov/mgg/global/relief/ETOPO1). (c) Simplified structural map of the North Makran domain and (d) geological cross-section showing the different tectonic units and their structural relationships (modified from Eftekhar-Nezhad et al. 1979; Burg, 2018; Samimi Namin, 1982, 1983). Box in (c) indicate the location of Figure 2a.

Figure 2: (a) Simplified geological maps and geological cross-section of the area to the south of Kahnuj city (see Fig. 1 and Supplementary Figure S1 for its location) showing the stratigraphic and structural setting of the sedimentary cover of the Band-e-Zeyarat ophiolite (based on Samimi Namin, 1983 and modified according to original fieldwork and photointerpretation with satellite images). (b) Stereographic plots showing mesoscale data for the structural elements of D1 and D2 phases from three distinct studied areas (Area 1, Area 2, and Area 3 represent A1, A2, A3 of Fig. 2a). The D1 and D2 deformative phases described by the diagrams are discussed in the text.

Figure 3: Schematic stratigraphic column (a) and field view of significant outcrops (b-f) of the transition zone sequence of the Band-e-Zeyarat ophiolite. The log (a) is reconstructed integrating data and observations along different sections in the studied area. The schematic position of significant biostratigraphic samples (e.g., MK23) and significant outcrops shown in (b-f) are also indicated in the log. b) panoramic view of the transition zone sequence with the indication of the main stratigraphic boundaries (white lines) between the different bodies; c) a close-up photo of pillow basalts (hammer for scale); d) pillow breccia showing clasts of limestone (hammer for scale); e) disrupted beds of interpillow limestone (indicated by white lines) embedded within the pillow breccia (hammer for scale); f) close-up view of the stratigraphic relationships between pillow lava flows and pelagic sedimentary rocks interlayered within the transition zone sequence (white line indicate the stratigraphic contacts; hammer in the top centre for scale).

Figure 4: Schematic stratigraphic column (a) and field view and microphotographs of significant outcrops (b-i) of the sedimentary cover of the Band-e-Zeyarat ophiolite. The column is reconstructed integrating data and observations along different sections in the studied area. The schematic position of significant biostratigraphic samples (e.g., MK408) and the stratigraphic position of Figures 4b-i are indicated in Figure 4a: b) close-up view of alternating thin beds of cherty limestone in the cherty limestone member (hammer for scale); c) medium to thin beds of alternating marls and limestones within the lower part of limestone and marls member (hammer for scale); d) tens of metric thick body of amalgamated arenitic turbidites interlayered within the upper part of the limestone and marl member (white line indicated the contacts of the body); e) photomicrograph of medium- to coarse-grained arenite from the amalgamated arenites in the limestone and marl member (crossed polarized light); f) alternating greyish to pinkish marls horizons of the varicoloured marls member (hammer for scale); g) medium beds of volcaniclastic turbidites within the upper part of the limestone and marls member (hammer for scale); h)

photomicrograph of the volcaniclastic turbidite composed of volcanic fragments (v), feldspar, and greenish volcanic glass (plane polarized light); i) photomicrograph of the volcaniclastic arenite showing a fragment of brown volcanic glass (g) with complex shape indicating an early soft-clast deformation (plane polarized light).

Figure 5: Distribution of selected calcareous nannofossil taxa recognized in the Band-e-Zeyarat ophiolite sedimentary cover, with calcareous nannofossil zones and events after Sissingh (1977), chronostratigraphy and age of the stage boundaries after Gradstein et al. (2012).

Figure 6: Relationships between dykes and sills and the sedimentary cover; the schematic position of significant outcrops shown in (a-b) are indicated in the Fig. 4a: a) crosscutting relationships between a basaltic dyke and the bedding of the limestone and marls member (hammer for scale). Rose diagram showing representative orientation of the basaltic dykes is also shown in the upper right of the figure; b) close-up view of the intrusive contact (white line) between a tabular sill and limestone in the limestone and marl member (hammer for scale); c) photomicrographs of the intrusive contact between a basaltic sill (at the bottom) and marl (at the top). Close to the contact reduction of the grain size of the sill and recrystallization of the marl are observed.

Figure 7: Geochemical diagrams for the dykes and sills intruding the sedimentary cover of the Band-e-Zeyarat ophiolite: (a) N-MORB normalized incompatible element patterns and (b) Chondrite-normalized rare earth element patterns. Normalizing values are from Sun and McDonough (1989). Compositions of E-MORB magmatic rocks from the magmatic sequence of the Band-e-Zeyarat ophiolite are from Barbero et al. (2020a) and are shown with grey fields; (c) N-MORB normalized Th vs. Nb discrimination diagram of Saccani (2015). Vectors indicate the trends of compositional variations due to the main petrogenetic processes. Abbreviations, AFC: assimilation-fractional crystallization; OIB-CE: ocean island-type (plume-type) component

enrichment; FC: fractional crystallization; MORB: mid-ocean ridge basalt; N-: normal type; E-: enriched type; P-: plume type; D-: depleted type; IAT: island arc tholeiite; CAB: calc-alkaline basalt; AB: alkaline oceanic within-plate basalt; MTB: medium titanium basalt. Normalizing values, as well as the composition of typical N-MORB (white star), E-MORB (grey star), and OIB (black star) are from Sun and McDonough (1989); (d) Nb/Yb vs. TiO_2/Yb diagram (Pearce, 2008). The compositional fields for plume-related Iceland basalts, plume-proximal Mid-Atlantic ridge (MAR) basalts, and Reykjanes Ridge basalts are shown for comparison (data from Hanan et al., 2000; Pearce, 2008). Abbreviations: OIB: ocean island basalt; Th: tholeiitic; Alk: alkaline; N: normal; E: enriched, MORB: mid-ocean ridge basalt. Compositions of magmatic rocks from the magmatic sequence of the Band-e-Zeyarat ophiolite shown in c) and d) are from Barbero et al. (2020a).

Figure 8: a) D_1 close folds showing axial planar foliation S_1 (indicated by light blue lines). The folded bedding S_0 is indicated by red lines; b) overturned SW-verging sub-isoclinal D_1 folds (red arrow indicate younging direction; red line the bedding) characterized by the refraction of the S_1 foliation in the hinge zone as a consequence of the competence of the deformed beds; c) structural relationships between S_1 foliation (light blue line) and S_0 bedding (red line) along the limbs of a multi-metric isoclinal folds; d) asymmetric D_1 fold with long and short limb indicating SSW vergence (red arrow indicate younging direction of the bedding); (e) mesoscale D_2 asymmetric open folds that deform the bedding S_0 (white lines). D_2 axial surface is indicated by green lines; f) D_2 folds (green lines indicate D_2 axial surfaces) deforming the D_1 axial planes (light blue lines). Mesoscale hinges of D_1 folds are marked by white lines that indicate the bedding S_0; g) D_2 open folds deforming D_1 folds producing Type 3 interference pattern (white lines are bedding S_0; light blue line indicate D_1 axial surfaces; green line D_2 axial surfaces) h) hinge zone of a D_2 open fold showing spaced cleavage representing the axial planar foliation.

Figure 9: a) close-up view of paraconglomerate alternated with tabular turbiditic arenite (hammer for scale); b) stereographic plot showing representative data of strike-slip fault systems and slikenlines; c) D3 gentle folds associated with the strike-slip faulting and deforming the sedimentary cover of the Band-e-Zeyarat ophiolite (black lines represent the folded bedding, blue line the axial plane; hammer for scale); d) stereographic projection of the structural elements (axial planes and axes) of the folds of the D3 deformation phase.

Figure 10: (a) Conceptual cartoon showing the evolutionary steps from mid-ocean ridge to the deformation in the Makran Accretionary Wedge that have been reconstructed for the oceanic lithosphere preserved in the Band-e-Zeyarat ophiolite. The three distinct steps described in the text are indicated by the different ages; b-c) schematic stratigraphic reconstructions for the deposition of the sedimentary cover of the Band-e-Zeyarat ophiolite during both the mid-ocean ridge setting (b) and the travelling away from the mid-ocean ridge toward the Makran convergent margin (c).

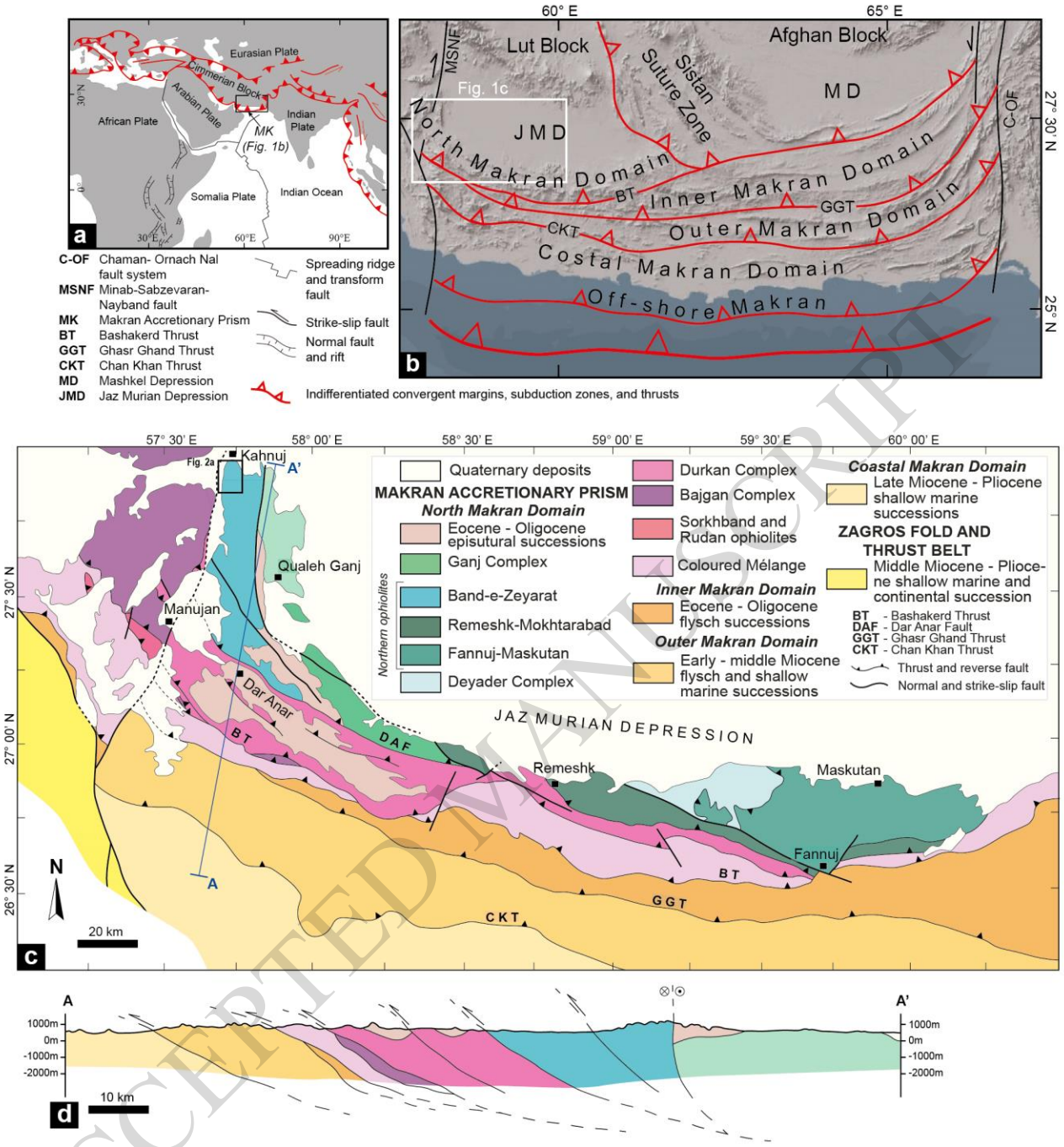

Figure 01 - Barbero et al., *(width 180 mm)*

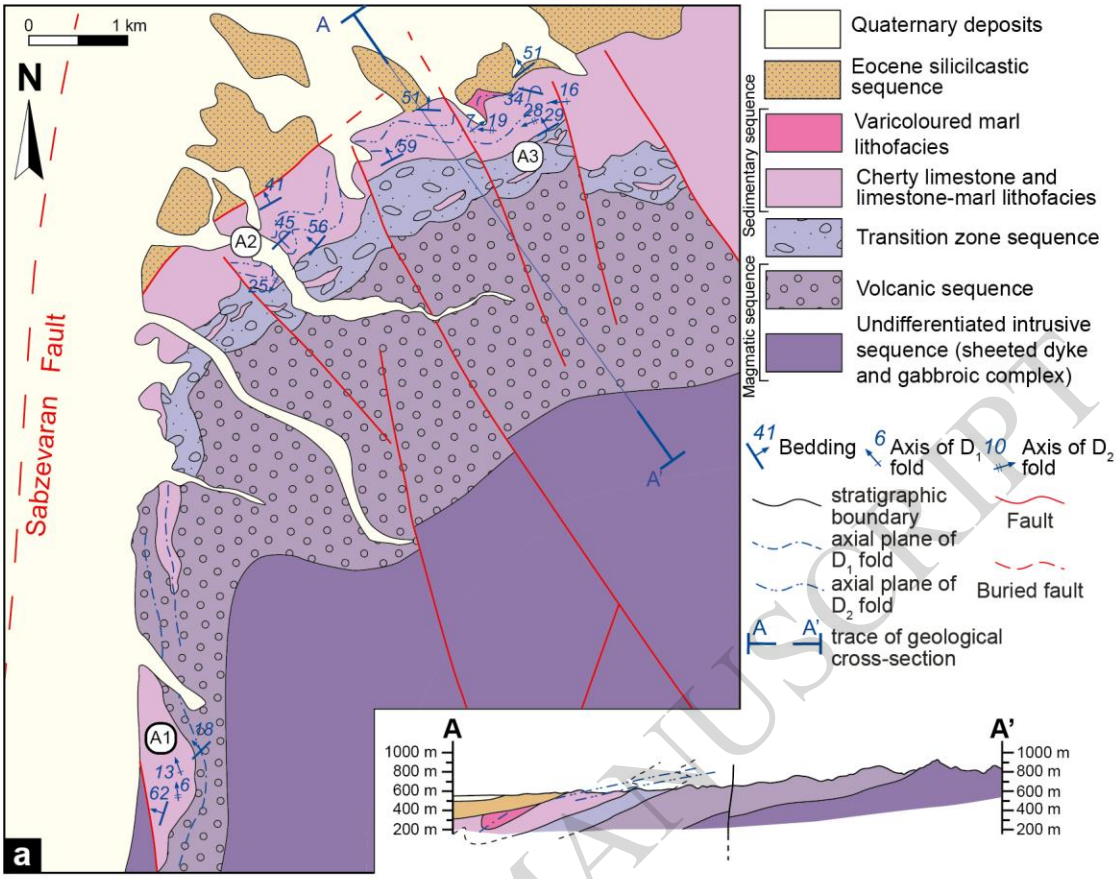

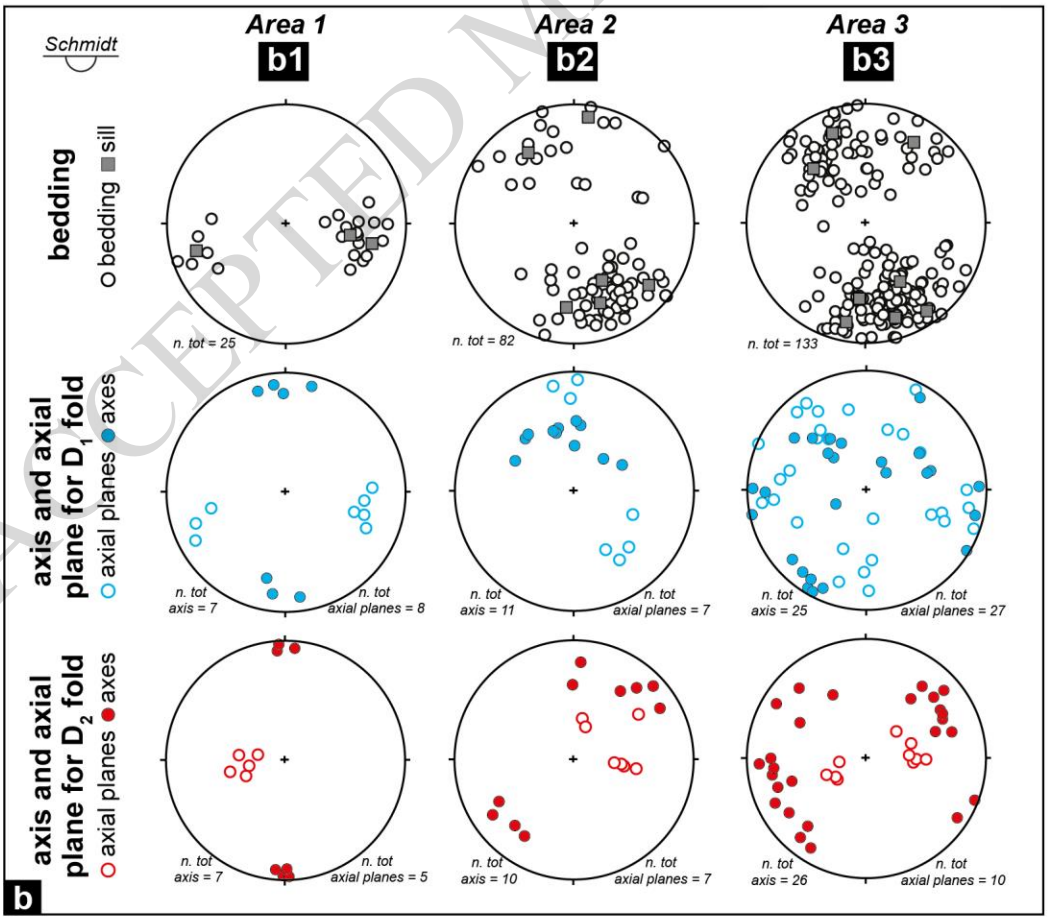

Figure 2 - Barbero et al., *(width 155 mm)*

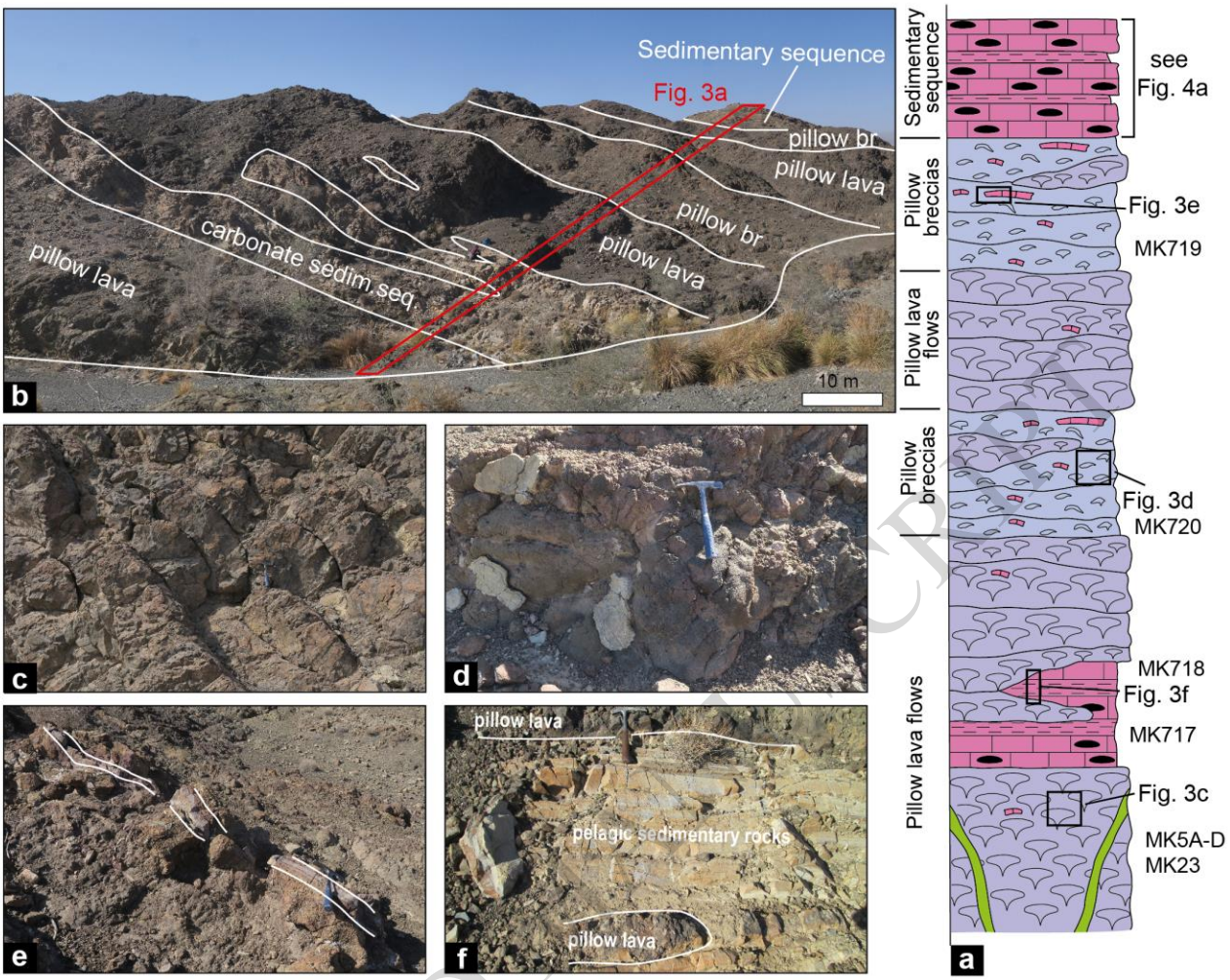

Figure 3 - Barbero et al., *(width 190 mm)*

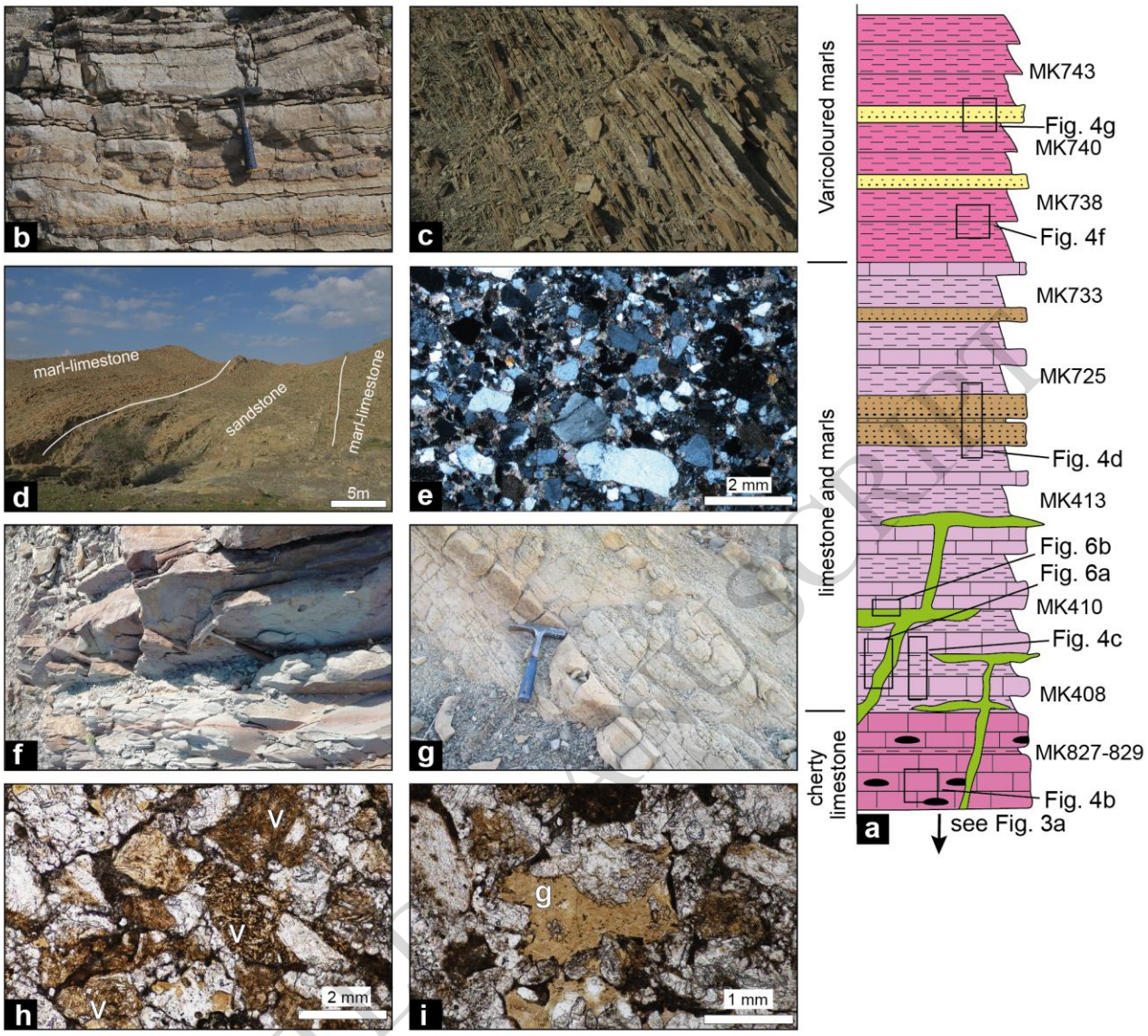

Figure 4 - Barbero et al., *(width 175 mm)*

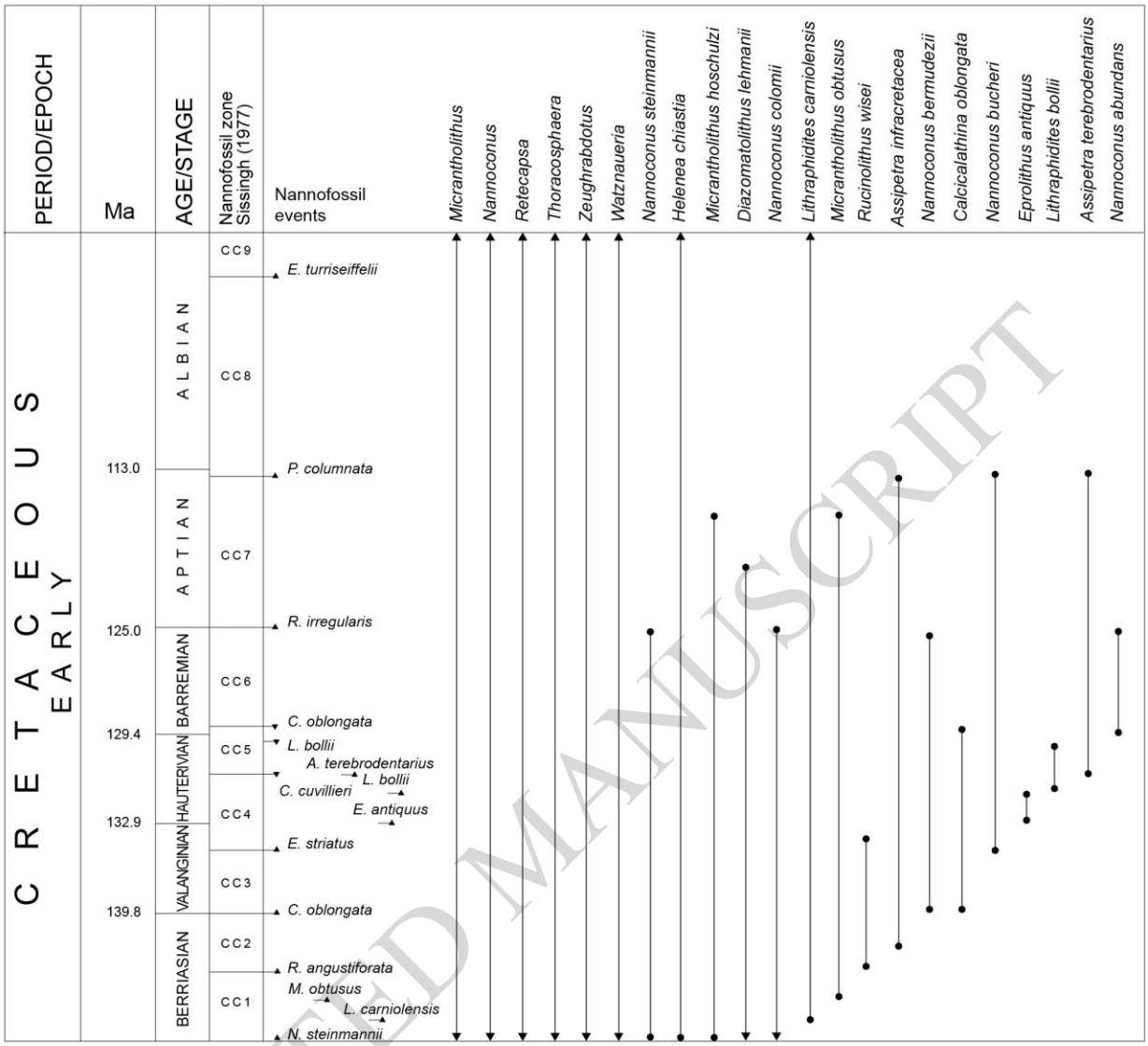

Figure 5 - Barbero et al., *(width 168 mm)*

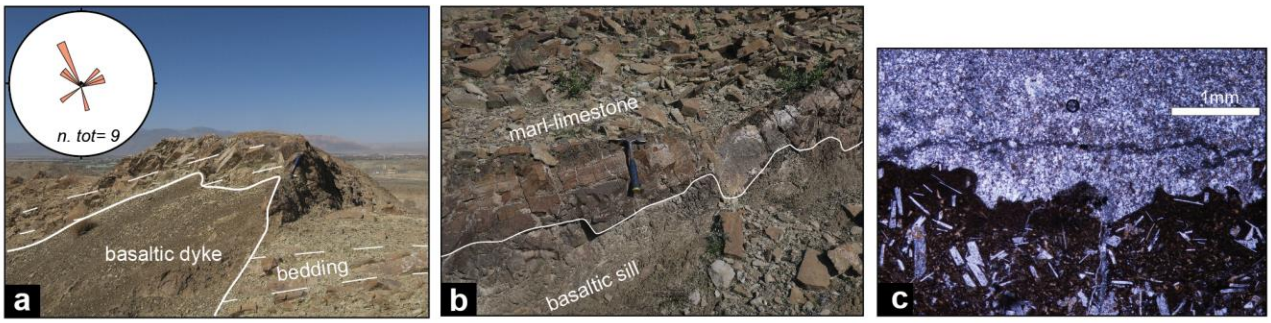

Figure 6 - Barbero et al., *(width 178 mm)*

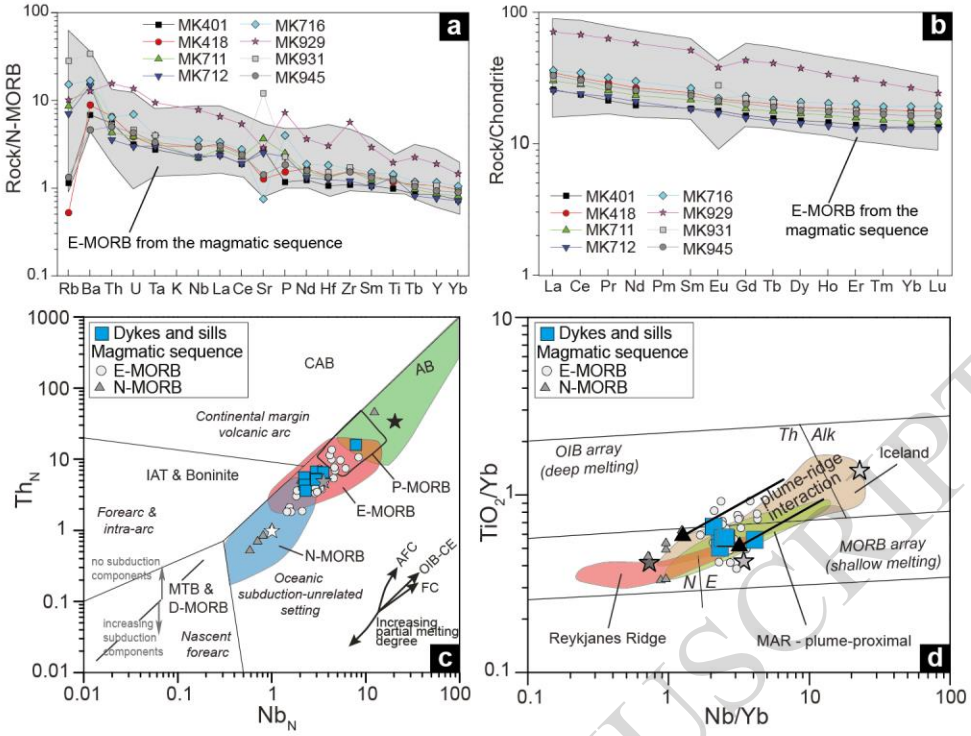

Figure 7 - Barbero et al., *(width 130 mm)*

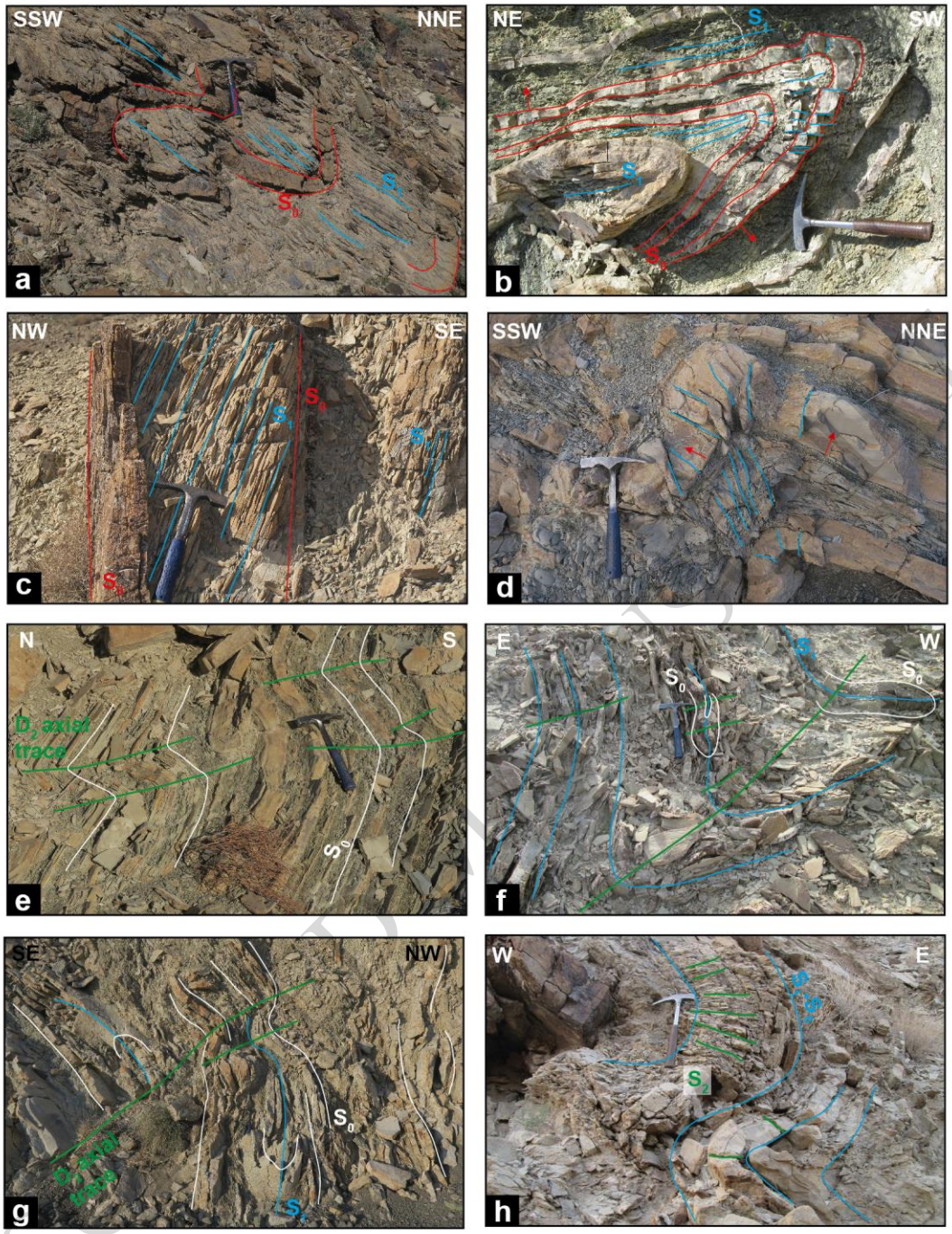

Figure 8 - Barbero et al., *(width 141 mm)*

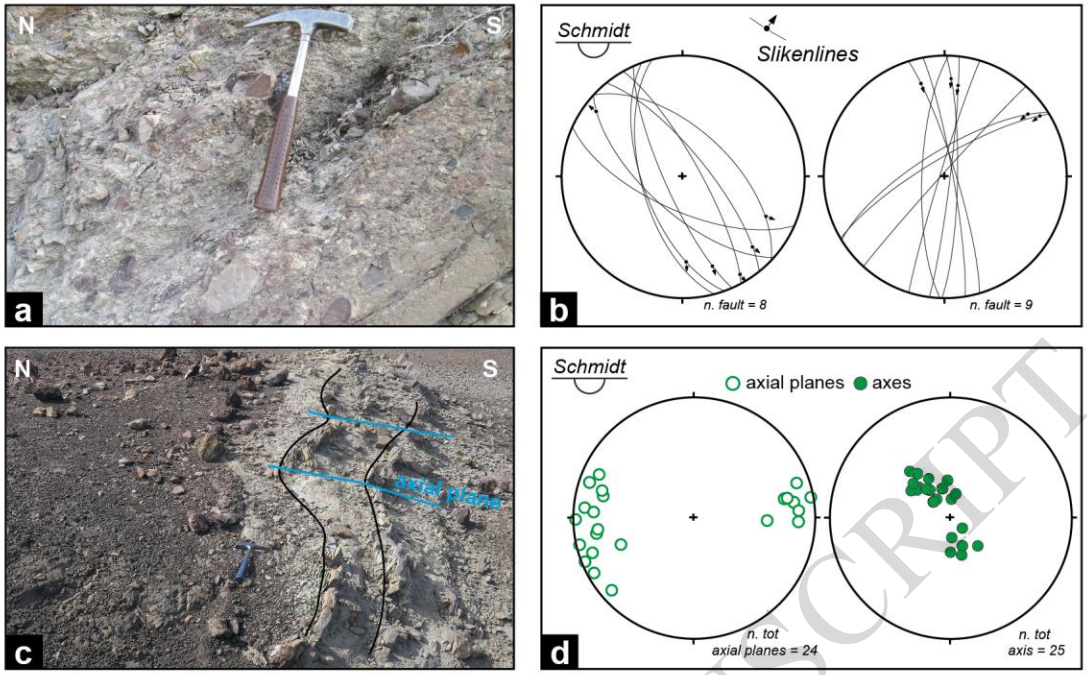

Figure 9 - Barbero et al., *(width 146 mm)*

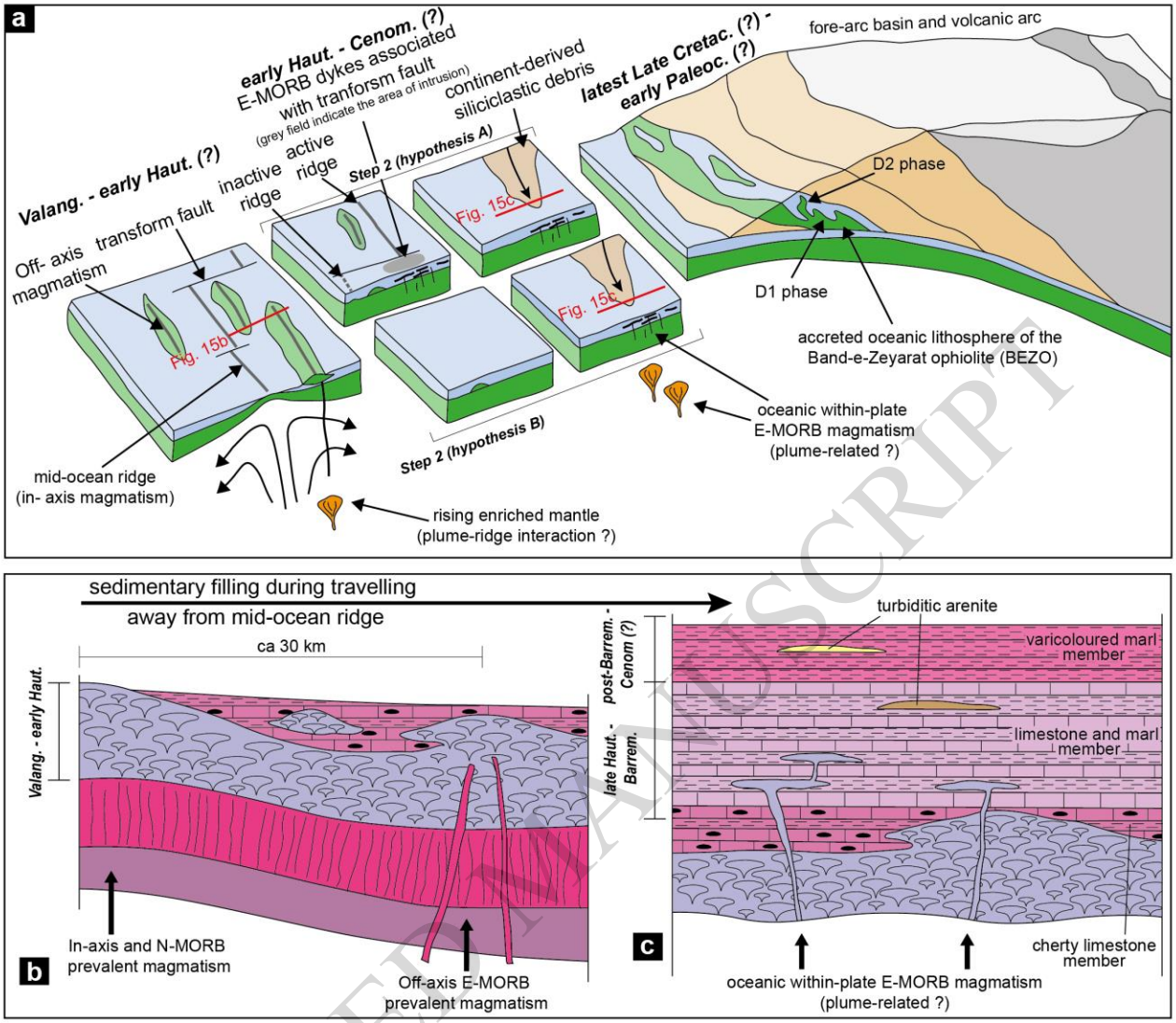

Figure 10 - Barbero et al., *(width 190 mm)*

Table 1

Sample	MK401	MK418	MK711	MK712	MK716	MK929	MK931	MK945
Rock	basalt	basalt	basalt	basalt	basalt	Fe-basalt	basalt	basalt
Texture	porphyritic	sub-ophitic	sub-ophitic	porphyritic	porphyritic	sub-ophitic	sub-ophitic	sub-ophitic
Type	dyke	sill	dyke	dyke	dyke	sill	sill	sill
XRF analyses:								
SiO_2	53.91	49.40	51.10	52.30	53.38	45.45	48.41	42.06
TiO_2	1.26	1.43	1.60	1.64	1.82	2.32	1.60	1.47
Al_2O_3	14.81	15.28	15.48	14.41	14.02	11.77	14.63	13.27
Fe_2O_3	1.23	1.13	1.11	1.33	1.14	1.76	1.40	1.26
FeO	8.21	7.51	7.38	8.89	7.58	11.75	9.01	8.41
MnO	0.13	0.13	0.18	0.28	0.23	0.14	0.20	0.15
MgO	7.14	7.83	10.53	10.31	4.74	10.66	10.15	11.08
CaO	9.22	9.58	4.92	3.45	8.74	5.82	8.44	11.58
Na_2O	3.23	2.11	3.18	3.15	5.28	1.79	2.01	2.70
K_2O	0.05	0.00	0.34	0.26	1.10	0.09	1.13	0.06
P_2O_5	0.14	0.17	0.28	0.26	0.47	0.80	0.26	0.20
LOI	0.71	5.48	3.84	3.45	1.13	7.66	2.66	7.89
Total	100.05	100.04	99.93	99.73	99.63	100.02	99.91	100.12
Mg#	60.8	65.0	71.8	67.4	52.7	61.8	66.7	70.1
Zn	37	53	43	37	63	136	55	53
Cu	45	55	54	58	48	15	49	51
Sc	26	24	28	24	24	14	25	23
Ga	17	20	18	15	17	24	18	15
Ni	66	70	93	74	55	19	51	71
Co	46	39	44	42	43	33	43	48
Cr	150	148	191	177	145	5	200	175
V	247	245	235	239	219	125	233	261
Ba	44	57	102	95	109	83	221	30
Pb	9	9	9	9	8	8	8	9
ICP-MS analyses:								
Rb	0.648	0.295	4.91	4.04	8.76	5.81	16.3	0.754
Sr	254	117	334	231	68.5	263	1113	130
Y	23.9	30.2	24.6	21.7	33.1	53.6	30.3	26.5
Zr	82.0	117	118	90.9	126	427	130	116
La	6.10	8.16	7.10	6.00	8.53	16.7	7.42	7.80
Ce	14.4	19.2	17.2	14.6	21.1	41.1	17.6	18.4
Pr	2.02	2.76	2.40	2.16	3.01	5.98	2.56	2.60
Nd	9.13	12.4	10.9	9.77	13.9	27.0	11.8	11.8
Sm	2.83	3.73	3.29	2.80	4.03	7.81	3.65	3.53
Eu	1.03	1.27	1.19	0.983	1.28	2.20	1.61	1.23
Gd	3.35	4.30	3.77	3.21	4.70	8.80	4.54	4.12
Tb	0.582	0.746	0.658	0.550	0.802	1.53	0.767	0.705
Dy	3.81	4.79	4.28	3.61	5.26	9.47	4.93	4.54
Ho	0.823	1.04	0.932	0.771	1.15	1.90	1.06	0.991
Er	2.30	3.01	2.59	2.15	3.30	5.13	2.94	2.81
Tm	0.342	0.458	0.385	0.334	0.486	0.732	0.442	0.425
Yb	2.26	3.00	2.51	2.20	3.25	4.51	2.88	2.76
Lu	0.339	0.452	0.369	0.327	0.489	0.611	0.440	0.415
Nb	5.26	7.00	5.28	5.42	8.40	18.6	7.05	7.03
Hf	2.21	2.87	2.73	2.61	3.81	6.31	3.16	2.78
Ta	0.370	0.413	0.447	0.406	0.536	1.27	0.538	0.448
Th	0.673	0.805	0.526	0.435	0.789	1.92	0.643	0.618
U	0.151	0.185	0.185	0.143	0.334	0.657	0.221	0.205
$(La/Yb)_N$	1.93	1.95	2.03	1.95	1.88	2.66	1.85	2.02
$(Sm/Yb)_N$	1.39	1.38	1.45	1.41	1.38	1.93	1.41	1.42